Ore Geology Reviews 80 (2017) 800–827

Contents lists available at ScienceDirect

Ore Geology Reviews

journal homepage: www.elsevier.com/locate/oregeorev

The Mesozoic magmatic sources and tectonic setting of the Zijinshan mineral field, South China: Constraints from geochronology and geochemistry of igneous rocks in the Southeastern Ore Segment

Gan Duan [a,d], Huayong Chen [a,b,*], Pete Hollings [c], Jinping Qi [e], Chao Xu [a,d], Shuang Zhang [a], Bing Xiao [a,d], Guangyong Liu [e], Jianmin Liu [e]

[a] Key Laboratory of Mineralogy and Metallogeny, Guangzhou Institute of Geochemistry, Chinese Academy of Sciences, Guangzhou 510640, China
[b] State Key Laboratory of Geological Processes and Mineral Resources, China University of Geosciences, Wuhan, Hubei 430074, China
[c] Department of Geology, Lakehead University, 955 Oliver Road, Thunder Bay, Ontario P7B 5E1, Canada
[d] University of Chinese Academy of Sciences, Beijing 100049, China
[e] Zijinshan Mining Group Co. Ltd., Shanghang 364200, Fujian, China

ARTICLE INFO

Article history:
Received 25 April 2016
Received in revised form 18 August 2016
Accepted 20 August 2016
Available online 23 August 2016

Keywords:
Zijinshan mineral field
Southeastern ore segment
Zircon U–Pb dating
Molybdenite Re-Os
Geochemistry
Tectonic evolution

ABSTRACT

The Zijinshan mineral field is a large porphyry-epithermal Cu—Au—Mo—Ag ore system located in the southwestern Fujian Province, China. The Southeast (Cu—Mo) Ore Segment (SOE) is a newly discovered section located in the southeastern portion of the Zijinshan mineral field. Zircon U—Pb and molybdenite Re—Os ages, as well as the geochemical compositions of intrusive and volcanic rocks and zircon Hf isotope data are used to constrain the timing, petrogenesis, tectonic setting and the relationship between magmatism and metallogenesis in the SOE and Zijinshan mineral field.

Major and trace element geochemistry indicates that igneous rocks from SOE are mainly shoshonitic granitoids that are LILE enriched (Rb, Ba, Th, U) with HFSE depletion (Nb, Ta, Zr, Hf and Y), indicating a subduction related setting. New U—Pb zircon analyses yield weighted mean ages of ca. 160 Ma for the Caixi pluton, ca. 110 Ma for the Sifang granodiorite, ca. 107–105 Ma for the Luoboling granodiorite porphyry, ca. 105 Ma for the quartz diorite porphyry, ca. 108–105 Ma for the dacite porphyry, ca. 98 Ma for the rhyodacite, and 97 Ma for the rhyolite in the SOE. These dates, integrated with previous geochronological data, indicate that there were two main magmatic events in this area: (1) a Middle to Late Jurassic event (165–150 Ma), and (2) a Cretaceous event (110–95 Ma) which can be further divided into two groups, i.e., the late Early Cretaceous event (110–105 Ma) and the early Late Cretaceous event (100–95 Ma). The late Early Cretaceous intrusions contain higher $\varepsilon_{Hf}(t)$ values (0.1 to −3.6), with T_{DM2} varying from 1.4 to 1.0 Ga, which may come from mixing between crustal and subduction-related mantle derived melts in contrast to the Middle to late Jurassic intrusions that may come from the partial melting of the Cathaysia Block basement. The early Late Cretaceous intrusions display a broader range of $\varepsilon_{Hf}(t)$ values (−0.9 to −9.4), with T_{DM2} varying from 1.8 to 1.2 Ga, suggesting a similar source to the late Early Cretaceous rocks but with more crustal material.

The molybdenite Re—Os ages for mineralization range from 110 Ma to 105 Ma, consistent with ages of the late Early Cretaceous rocks. Zircon trace elements analyses imply that the early Late Cretaceous rocks (Ce^{4+}/Ce^{3+} = 113–1800) are characterized by higher oxygen fugacity with higher mineralization potential than the late Early Cretaceous (Ce^{4+}/Ce^{3+} = 9–545) and the Middle to Late Jurassic rocks. Variability in ages, geochemistry and oxygen fugacity indicate that the Middle to Late Jurassic magmatic event represents pre-mineralization intrusions whereas the late Early Cretaceous is syn-mineralization and the early Late Cretaceous intrusions post-mineralization. We propose that both the Middle to Late Jurassic and the Cretaceous magmatic events may relate to the subduction of the Pacific slab, and the changing direction of the subducted slab may result in the different sources for the two magmatic events.

* Corresponding author at: Key Laboratorye of Mineralogy and Metallogeny, Guangzhou Institute of Geochemistry, Chinese Academy of Sciences, Guangzhou 510640, China.
E-mail address: huayongchen@gig.ac.cn (H. Chen).

http://dx.doi.org/10.1016/j.oregeorev.2016.08.016
0169-1368/

1. Introduction

The Zijinshan porphyry-epithermal Cu—Au—Mo—Ag ore system is located in the southwestern Fujian Province of China (Fig. 1; So et al., 1998; Gao, 1999; Zhang et al., 2001, 2003; Zhong et al., 2014). By the end of 2008, the proven reserves in the Zijinshan mineral field were 323 t Au (grading ca. 0.5 g/t), 2.36 Mt Cu (ca. 0.45%), 1554 t Ag (20 to 156 g/t), 4647 t Mo (0.032%), 6279 t Pb (3.47%), and 1747 t Zn (3.75%) (Zhong et al., 2014). Since the discovery of the Zijinshan Cu—Au deposit in 1988, many researchers have investigated the geology, geochemistry, alteration, mineralization, and characteristics of the mineralizing fluids (Zhang et al., 1996; So et al., 1998; Zhang et al., 2003, 2005; Liu and Hua, 2005; Chen et al., 2011; Zhong et al., 2011). Despite this work there is still confusion as to the precise ages of different plutons. For example, the Rb—Sr ages for the Zijinshan granite complex (Zhang et al., 2001) are not reliable due to intensive alteration and mobility of the LILE. The geodynamic setting of the rocks and mineralization in the Zijinshan mineral field are also the subject of debate. Zhang et al. (2001) proposed that the Jurassic intrusions were emplaced in a compressional tectonic setting and the Cretaceous granodiorite and volcanic rocks in an extensional tectonic setting. Mao et al. (2002) further pointed out that the emplacement of the ca. 110 Ma Sifang granodiorite resulted from upwelling of the asthenosphere under the South China Block, whereas others suggested that Cretaceous rocks formed in a subduction-related tectonic setting (Jiang et al., 2013; Li and Jiang, 2014a, 2014b; and Li et al., 2015). Consequently, more detailed studies of these igneous rocks are necessary to establish a comprehensive tectonic and metallogenic model for the Zijinshan mineral field.

The newly discovered Southeast Ore Segment (SOE) of the Zijinshan district, located between the Zijinshan high sulfidation epithermal Cu—Au deposit and the Luoboling porphyry Cu—Mo deposit, includes most of the rock types in the Zijinshan mineral field. The currently explored SOE is a Cu—Mo deposit with estimated reserves of about 0.1 Mt Cu metal at an average grade of 0.4% and 3000 t Mo at an average grade of 0.012% (Zijin Mining Group Co., 2014). The SOE is spatially associated with the Luoboling granodiorite porphyry and Sifang granodiorite, which are also spatially associated with the Luoboling porphyry deposit, but distinct from the Zijinshan Cu—Au deposit that is hosted by the Zijinshan granite complex (So et al., 1998). Based on a molybdenite Re—Os isotopic isochron age of 104.9 ± 1.6 Ma, the Luoboling porphyry Cu—Mo deposit was interpreted to be coeval with the Luoboling pluton (Liang et al., 2012). But the absence of good geochronology means that the link between plutonism and the Cu—Mo mineralization in the SOE is unclear. The location of the SOE between the major Zijinshan Cu—Au and Luoboling Cu—Mo deposits offers an excellent chance to study the genetic relationship between the mineralization and the various intrusions in the area and to utilize this to investigate the tectonic setting during mineralization.

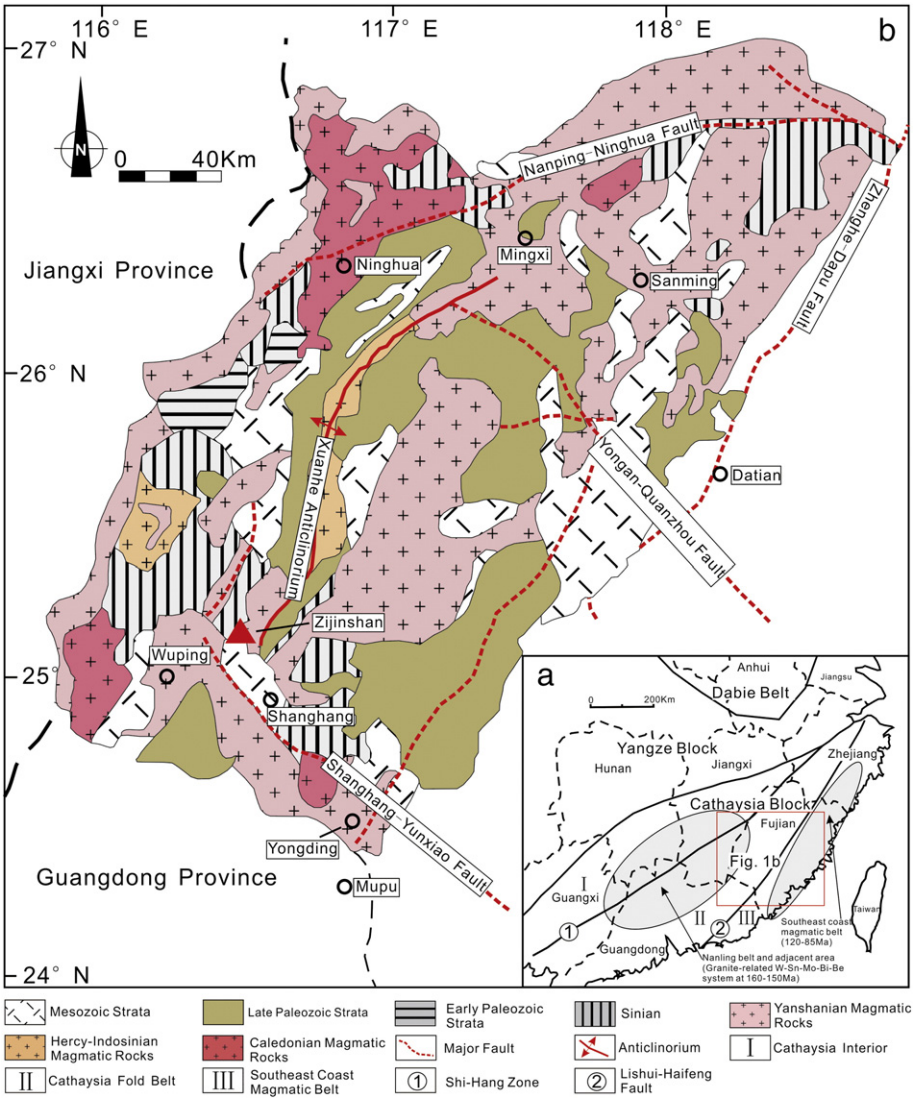

Fig. 1. (a) Tectonic map showing the location of the study area (modified after Mao et al., 2013). (b) Regional geological map of Fujian Province (modified after Zhong et al., 2011).

Precise new zircon U—Pb ages, geochemistry, zircon in-situ Hf isotope data from igneous rocks, and Re—Os ages of molybdenite from the SOE, are used to establish a more accurate sequence of magmatism at Zijinshan mineral field, discuss the petrogenesis of the igneous rocks, and build a tectonic model for both the magmatic and the ore-forming events.

2. Geological setting

2.1. Regional geology

The South China Block, which is located in the south part of China, includes the Yangtze and Cathaysia blocks (Fig. 1a). The Cathaysia Block can be divided into the Cathaysia Interior, the Cathaysia Fold Belt, and the Coastal Magmatic Belt, which are separated by the Shi-Hang Zone and Lishui-Haifeng Fault (Fig. 1a; Chen et al., 2008). The Mesozoic geology of the Cathaysia Block is characterized by widespread Jurassic to Cretaceous igneous rocks, consisting predominantly of granites and rhyolites and subordinate mafic lithologies (Li and Li, 2007). Mesozoic magmatism was concentrated in the Cathaysia Block with an oceanward increase in magmatic activity (Zhou et al., 2006). Triassic and Jurassic granitoids are primarily located in the inland region, whereas Cretaceous intrusions and volcanic rocks are mostly concentrated in the coastal region (Zhou and Li, 2000).

The Zijinshan mineral field is located in the Cathaysia Fold Belt on the northeastern margin of the Cretaceous Shanghang Volcanic Basin and at the intersection of the Xuanhe Anticline and the Shanghang-Yunxiao Fault (Fig. 1b). The transition from late Jurassic compression to the Early Cretaceous extension is supported by the nappe structure in northwestern Fujian (Zhang, 2014). The field consists of the Zijinshan high sulfidation (HS) epithermal Cu—Au deposit (So et al., 1998; Zhang et al., 2003), the Luoboling porphyry Cu—Mo deposit (Zhong et al., 2011), the Yueyang low sulfidation (LS) epithermal Ag—Au—Cu deposit (Lin, 2001; Liang et al., 2015), the Wuziqilong Cu deposit (Chen et al., 2011), the Ermiaogou Cu—Au deposit (Lin et al., 2012), and the Longjiangting Cu deposit (Zhang et al., 1996; Chen et al., 2015).

The exposed strata in the district consists of Neoproterozoic phyllite and fine-grained metasandstone (Louziba Formation) unconformably overlain by Devonian-Carboniferous clastic rocks and limestone (Tianwadong Group and Landi Group; Fig. 2). The Early Cretaceous volcanic rocks crop out in the northwest part of the district and in the Shanghang Volcanic Basin, where they unconformably overly the Louziba Formation, Tianwadong Group and Landi Group (Zhang et al., 2001). The Middle to Late Jurassic and Early Cretaceous magmatic rocks are the dominant units in the Zijinshan mineral field (Zhang et al., 2001; Chen et al., 2008; Jiang et al., 2013). The Middle Jurassic Zijinshan granite complex, which is mainly located in the southeastern part of the district, hosts the Zijinshan high sulfidation epithermal deposit (So et al., 1998), and comprises the Jingmei, Wulongsi, and Jinlongqiao plutons, with multiple phases that grade outward from coarse-grained to fine-grained granites (Zhang et al., 2001). Cross-cutting relationships show that the Wulongsi pluton intruded into the Jingmei pluton, and was intruded by the Jinlongqiao pluton (Zhang et al., 2001) consistent with the published U—Pb ages (ca. 165 Ma for the Jingmei pluton, ca. 164 Ma for the Wulongsi pluton, ca. 157 Ma for Jinlongqiao pluton; Jiang et al., 2013). The 150 Ma Late Jurassic Caixi monzogranite (Zhao et al., 2007; Yu et al., 2013) is located in the northeast area of the region and intruded into the Wulongsi pluton (Fig. 2; Mao et al., 2004). The ca. 110 Ma Early Cretaceous NNE-trending Sifang granodiorite (Jiang et al., 2013; Yu et al., 2013) crops out in the

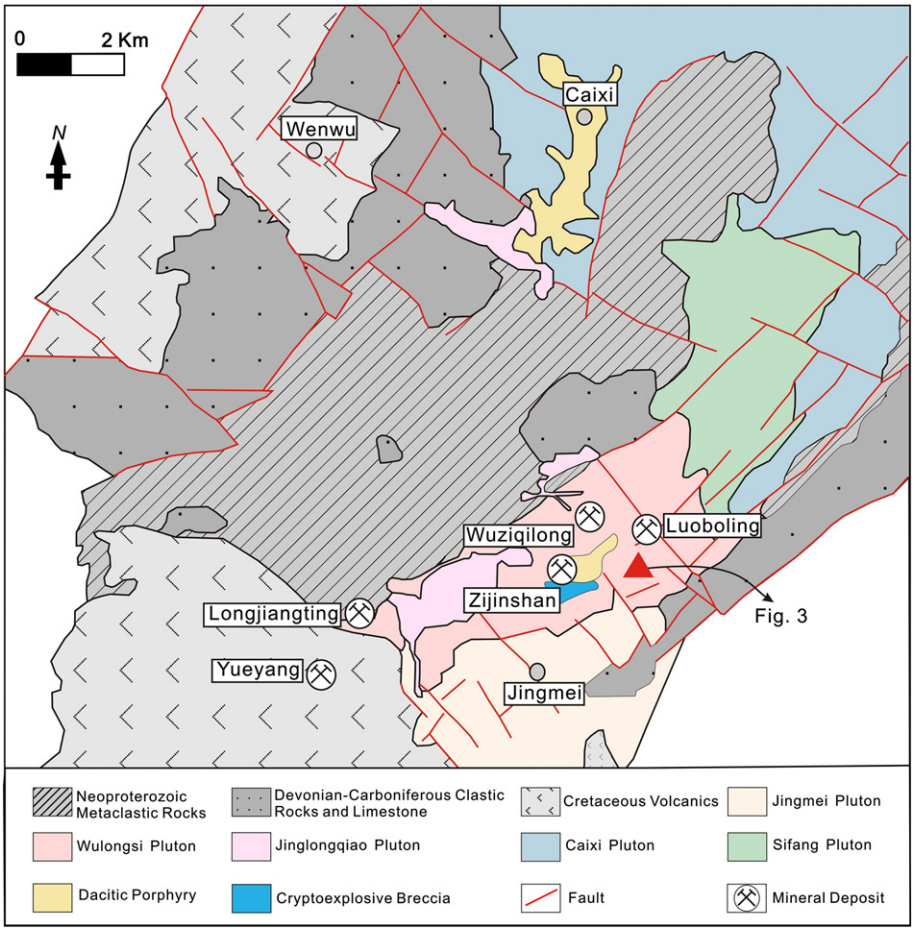

Fig. 2. Regional tectonic framework of the Zijinshan region (modified after Jiang et al., 2013).

northeast of the region, and was emplaced into Neoproterozoic metamorphic rocks, Devonian-Carboniferous clastic rocks and limestone, and the Wulongsi and Caixi plutons (Zhang et al., 2001). The Cretaceous Luoboling granodiorite porphyry is located in the northeast of the region and cuts the Sifang granodiorite (Fig. 2; Zhang et al., 2001). The Luoboling pluton has yielded ages ranging from ca. 105 Ma to ca. 97 Ma (Zhang et al., 2001; Huang et al., 2013).

Many Late Cretaceous intermediate to felsic dikes, including porphyritic quartz monzonite, porphyritic syenite, syenite, dacite porphyry, diorite and dolerite are present in the area where they cut the Sifang granodiorite, the Luoboling granodiorite porphyry, and the Zijinshan granite complex (Fig. 2).

2.2. Southeast ore segment geology

The SOE is located in the eastern part of the Zijinshan district, between the Zijinshan Cu—Au deposit and the Luoboling Cu—Mo deposit (Fig. 2). North east-, NNE-, and E-trending faults are very common in the study area (Fig. 3). The magmatic rocks in the SOE region are mainly Mesozoic and comprise the Wulongsi granite (part of the Zijinshan granite complex), the Sifang granodiorite, Luoboling granodiorite porphyry, Caixi monzogranite, quartz diorite porphyry, dacite porphyry, rhyodacite and rhyolite (Figs. 3 and 4).

These igneous rocks show clear temporal and spatial relationships in the SOE. The exposed plutons in the SOE are mainly the Wulongsi pluton and the Sifang pluton (Fig. 3). The Wulongsi pluton has been intruded by the Sifang pluton (Figs. 3 and 4) whereas the latter has been intruded by the Luoboling pluton at depth in the SOE (Fig. 4). In drill hole ZK4806, the Sifang granodiorite was enclosed by the Luoboling granodiorite porphyry on the cm-scale (Fig. 5a). In drill hole ZK3220 at about 90 m in elevation, the Caixi monzogranite was enclosed by the Luoboling pluton (Fig. 5b). Quartz diorite porphyry, rhyolite, dacite porphyry and the rhyodacite are emplaced as stocks in the SOE (Fig. 4). The quartz diorite porphyry was emplaced in the shallow part as stocks intruded into the Sifang granodiorite (Fig. 4). The Sifang pluton in contact with the quartz diorite porphyry and locally has a fragmented structure (Fig. 5c). Rhyolite, dacite porphyry and rhyodacite are subvolcanic rocks that outcrop in the SOE. The rhyolite cuts the Sifang granodiorite in drill holes ZK4806 and ZK5605 (Figs. 4 and 5d), and the dark minerals in the rhyolite were aligned parallel to the contact (Fig. 5e). The dacite porphyry intruded into the Sifang granodiorite (Fig. 4), and also into the Wulongsi pluton in drill hole ZK4017 (Fig. 5f). The rhyodacite is emplaced as an approximately two meter long unit that cuts the Luoboling pluton in dill hole of ZK3215 (not shown), indicating a late magmatism event at SOE and Zijinshan.

3. Igneous samples and petrography

Samples for this study were collected from eight different drill cores from the SOE (Table 1). Their petrographic characteristics are described below:

The Caixi monzogranite (Fig. 6a, b), is enclosed by the Luoboling porphyry in the deep part of drill hole ZK3220. It is pink in color with a coarse-grained texture, consisting of K-feldspar (~35%), plagioclase (~30%), quartz (~30%) and biotite (<5%), with accessory zircon, apatite and titanite.

The Wulongsi pluton (Fig. 6c, d), part of the Zijinshan granite complex, from drill hole ZK4806, has been subjected to alunite and dickite alteration as well as silification. The main rock forming minerals have been commonly altered to dickite or alunite, only leaving the shape of the original minerals (Fig. 6d).

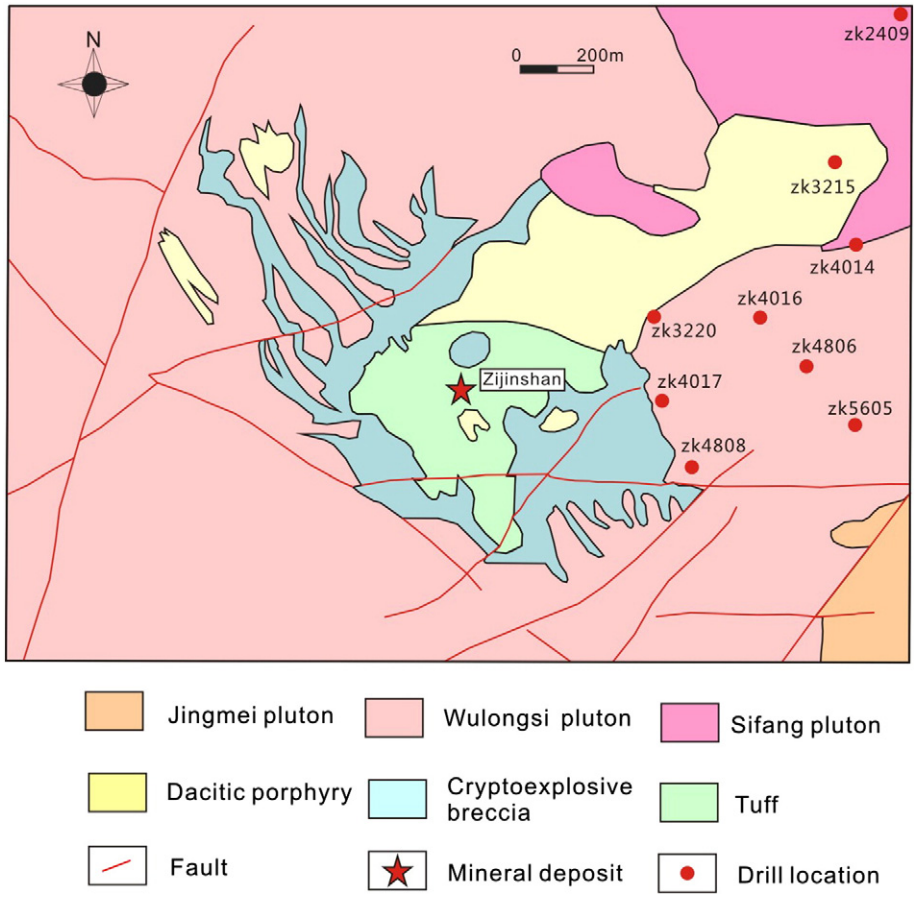

Fig. 3. Geologic map of the Southeast ore segment of Zijinshan Mineral field (modified from Zijin Mining Group Co., 2014).

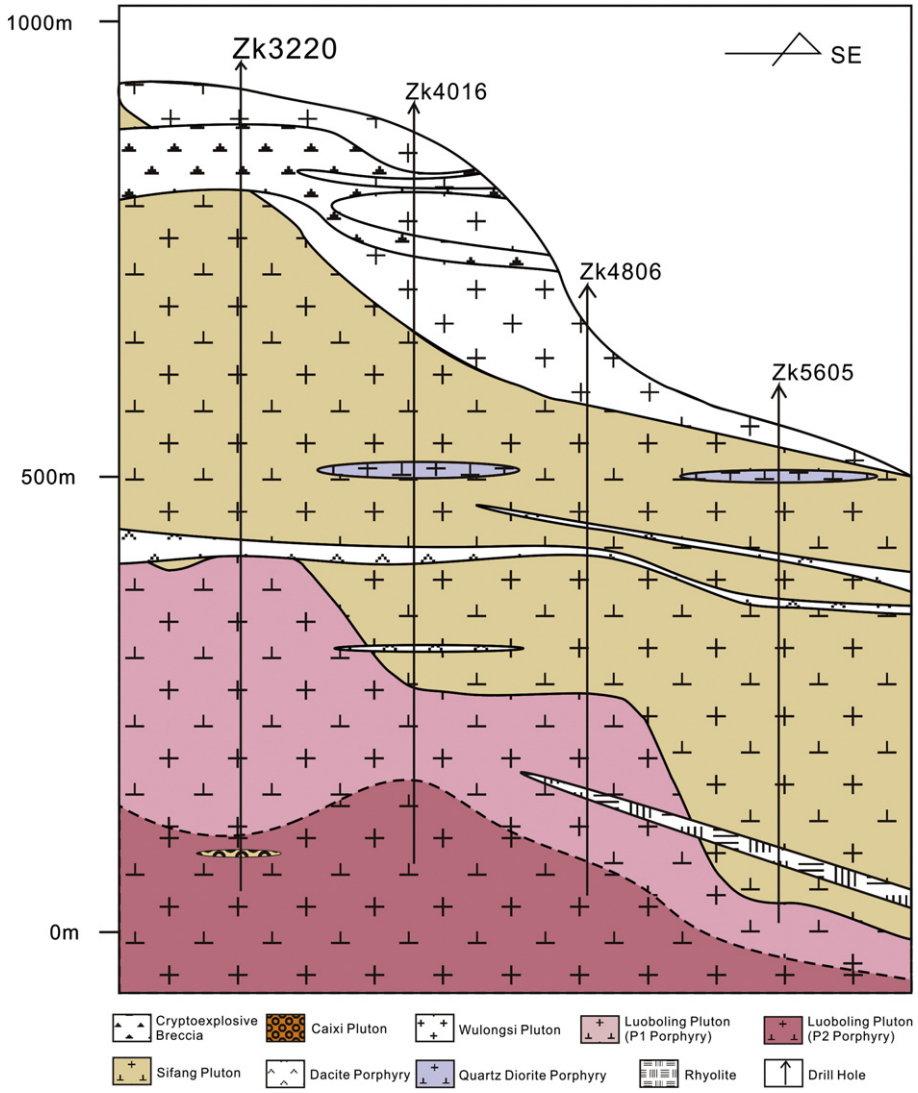

Fig. 4. The northeastern trending sketch profile of the SOE.

The fine- to medium-grained Sifang granodiorite (Fig. 6e, f) samples have been subjected to intensive dickite and sericite alteration, and as a result the mineral assemblages can only be approximately distinguished by the appearance of the residual crystal shapes. Based on previous studies, the fresh Sifang granodiorite (in the Zijinshan region) is composed of 0.2 to 5 mm plagioclase (~40%), quartz (~25%), K-feldspar (~20%), and biotite (~10%), with accessory minerals including titanite, apatite and zircon (Jiang et al., 2013).

The Luoboling granodiorite porphyry in the SOE can be subdivided into three types based on depth. At shallow depths (240 m to 50 m in drill hole ZK4806; Fig. 6g, h), it contains 1–5 mm phenocrysts of plagioclase (25%) and quartz (15%), with minor biotite (5%) and hornblende (5%). Minerals in the groundmass are generally <50 μm, and mainly comprise quartz (20%), K-feldspar (15%), plagioclase (10%) and biotite (5%). Accessory minerals include magnetite, apatite and zircon, and we define it as the P1 porphyry, which represents the shallow part of the Luoboling granodiorite porphyry. At greater depths (below 100 m in drill hole ZK3220; Fig. 6i, j), the groundmass is comprised of the same minerals as the P1 porphyry but they are considerably larger and up to 100 um distinguishing it from the P1 porphyry. Consequently we term this the P2 porphyry, which forms the intermediate portion of the Luoboling granodiorite porphyry. At depths below 160 m (drill hole ZK2409; Fig. 6k, l), the rock is more equigranular but with the same dominant mineralogy and it is termed the P3 porphyry, and is the deepest portion of the Luoboling granodiorite porphyry. The main alteration minerals in the Luoboling pluton are potassium feldspar, montmorillonite, chlorite, and calcite. The P1 porphyry is characterized by moderate sericite alteration of feldspar whereas the P2 and P3 porphyry are somewhat less altered when compared to the P1 porphyry, the Sifang and the Wulongsi plutons.

The quartz diorite porphyry was emplaced in the shallow parts of the SOE as stocks and cuts the Sifang granodiorite. The quartz diorite porphyry (Fig. 6m, n) is red in color, consisting of plagioclase (~10%), K-feldspar (~10%), quartz (~15%), and biotite (3%–5%) phenocrysts with a matrix of felsic aphanitic minerals. The dark minerals in the quartz diorite porphyry have been altered to chlorite but primary crystal shapes are preserved. The plagioclase and K-feldspar have been partially altered to montmorillonite (Fig. 6n).

The dacite porphyry was emplaced as stocks in the SOE and cuts both the Sifang granodiorite and the Wulongsi pluton. The dacite porphyry (Fig. 6o, p) is white in color, and has been intensely altered. Both the phenocrysts and the groundmass have been altered to the sericite and quartz with minor pyrite (Fig. 6p). There are at least two types of the dacite porphyry, one went through intense alteration, with only relic crystal shapes preserved; the other is less altered with primary phenocrysts minerals of quartz, biotite and plagioclase preserved. These two types of the dacite porphyry intruded in different positions in the SOE, with the intensively altered rocks above 50 m in the

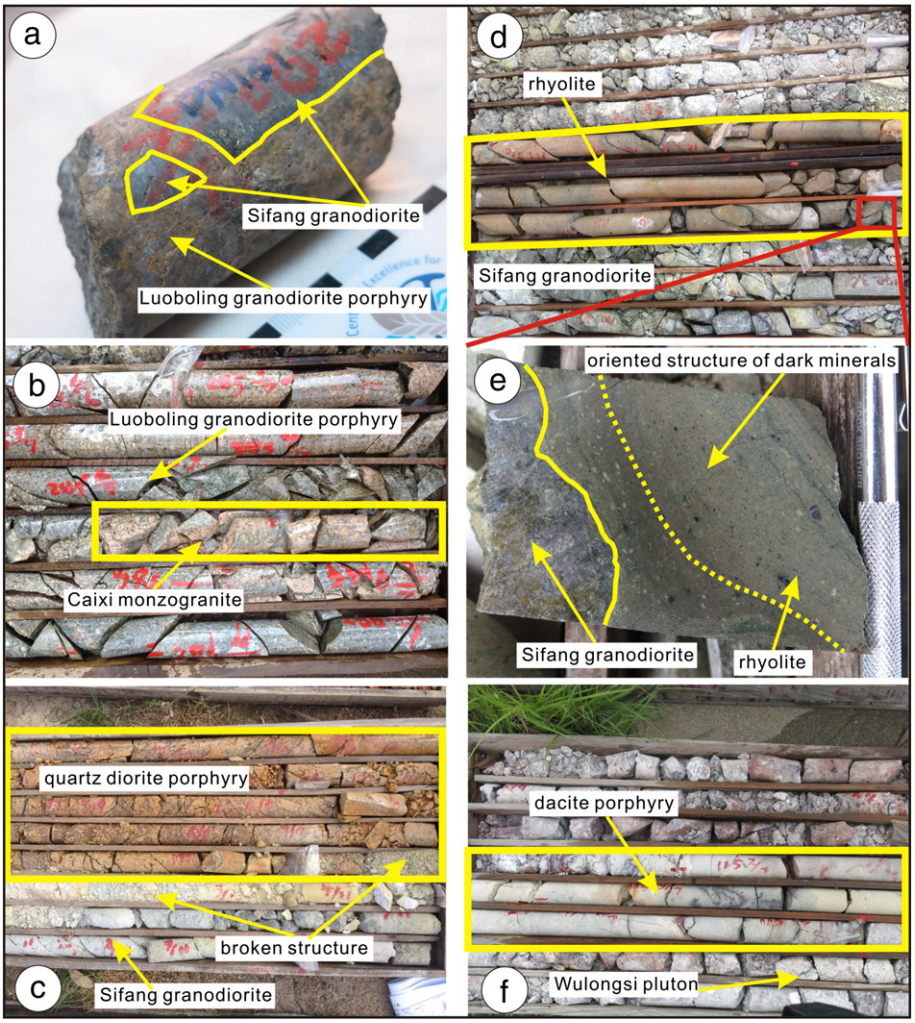

Fig. 5. Representative photographs showing the cross-cutting and contact relationships between the igneous rocks from the SOE. a) The Sifang granodiorite enclosed by the Luoboling granodiorite porphyry on the cm-scale in drill hole ZK4806 in the boundary between the Luoboling pluton and the Sifang granodiorite. b) The Caixi monzogranite enclosed by the Luoboling pluton in drill hole ZK3220. c) The Sifang pluton in contact with the quartz diorite porphyry locally has a fragmented structure in drill hole ZK4016. d) The rhyolite cutting the Sifang granodiorite in drill hole ZK5605. e) The dark minerals in the rhyolite are aligned along the contact between the rhyolite and the Sifang granodiorite in drill hole ZK5605. f) The dacite porphyry intruded into the Wulongsi pluton.

SOE and the less altered below 100 m in the SOE. In the intensive altered dacite porphyry the original minerals are pervasively replaced by sericite, quartz and dickite. Since these two kinds of dacite porphyry occur in different positions and have different degrees of alteration, we define the intensively altered dacite porphyry as D1 porphyry and the less altered dacite porphyry as D2 porphyry.

The rhyodacite was emplaced only locally in the SOE and intruded into the Luoboling pluton. The rhyodacite (Fig. 6q, r) is comprised of quartz (~15%) and plagioclase (~30) as phenocrysts in a groundmass of K-feldspar (~30%) microcrystals, exhibiting hyalopilitic texture (Fig. 6r). The rhyodacite has been intensively altered with montmorillonite and calcite replacing the K-feldspar.

Table 1
Sample locations.

Sample	Description	Location	Note
DN292	Medium-course-grained monzogranite	ZK3220-841 m	Caixi pluton
DN101	Medium-fine-grained granite	ZK4806-13 m	Wulongsi pluton
DN117	Granodiorite	ZK4806-356 m	Sifang pluton
DN011	Granodiorite	ZK4017-513 m	Sifang pluton
DN138	Granodiorite porphyry	ZK4806-538 m	Luoboling pluton
DN291	Granodiorite porphyry	ZK3220-880 m	Luoboling pluton
DN259	Granodiorite porphyry	ZK2409-595 m	Luoboling pluton
DN040	Dacite porphyry	ZK4014-30 m	
DN196	Dacite porphyry	ZK4808-136 m	
DN114	Dacite porphyry	ZK4806-197 m	
DN054	Quartz diorite porphyry	ZK5605-54 m	
DN090	Rhyolite	ZK5605-468 m	
DN178	Rhyodacite	ZK3215-366 m	

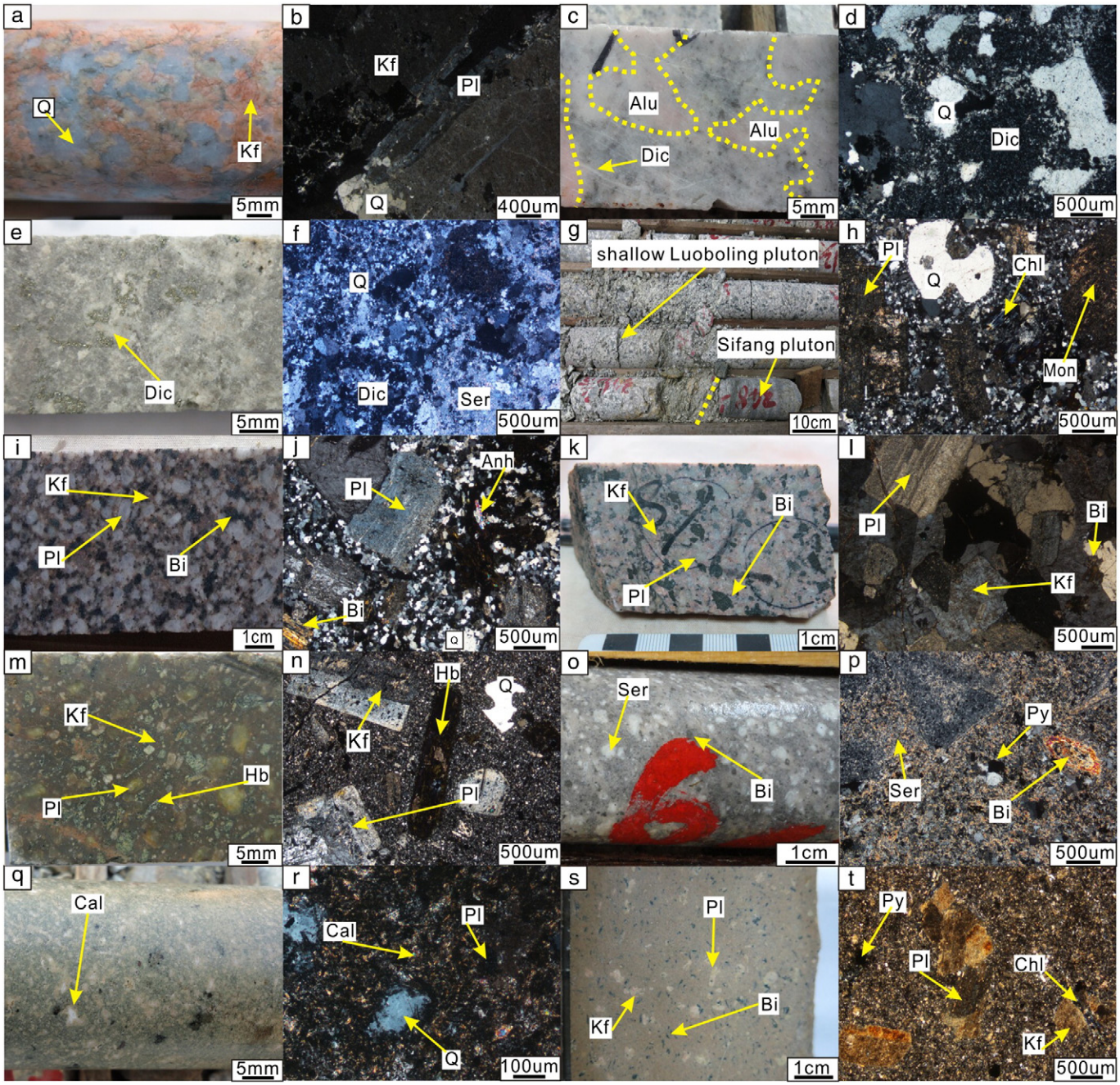

Fig. 6. Representative photographs and photomicrographs of the rock types in the southeast ore segment of the Zijinshan mineral field. a) Caixi monzogranite (drill-hole sample). b) Caixi monzogranite (transmitted light with crossed nicols). c) Wulongsi Medium-fine-grained granite was subjected to alunite alteration (polished surface). d) Wulongsi Medium-fine-grained granite (transmitted light with crossed nicols). e) Sifang granodiorite was subjected to dickite alteration (polished surface). f) Sifang granodiorite (transmitted light with crossed nicols). g) The boundary between the Sifang pluton and the shallow Luoboling pluton (P1 porphyry) (drill hole sample). h) The shallow Luoboling pluton (P1 porphyry) (transmitted light with crossed nicols). i) Deeper Luoboling pluton (P2 porphyry) (polished surface). j) Deeper Luoboling pluton (P2 porphyry) (transmitted light with crossed nicols). k) Deepest Luoboling pluton (P3 porphyry) (polished surface). l) Deepest Luoboling pluton (P3 porphyry) (transmitted light with crossed nicols). m) Quartz diorite porphyry with weak alteration (polished surface). n) Quartz diorite porphyry (transmitted light with crossed nicols). o) Dacite porphyry with weak alteration (drill hole sample). p) Dacite porphyry (transmitted light with crossed nicols). q) Rhyodacite with weak calcite alteration (drill hole sample). r) Rhyodacite (transmitted light with crossed nicols). s) Rhyolite (polished surface). t) Rhyolite (transmitted light with crossed nicols). Abbreviations in figures are based on Whitney and Evans (2010). Abbreviations: Hb = hornblende, Kf = K-feldspar, Pl = plagioclase, Chl = chlorite, Mon = montmorillonite, Dic = dickite, Ser = sericite, Py = pyrite, Qz = quartz Cal = calcite.

The rhyolite normally cuts the Sifang granodiorite in the SOE. The rhyolite (Fig. 6s, t) is generally porphyritic, consisting of K-feldspar (~20%), quartz (~25%), plagioclase (~15%), biotite (~10%), and hornblende (~5%) phenocrysts in a matrix of aphanitic felsic minerals. The mafic minerals have been weakly altered to chlorite, and the feldspars have been partially altered to montmorillonite.

4. Analytical methods

4.1. Zircon U—Pb geochronology and in-situ Hf isotopes

All the samples were crushed, sieved and the heavy mineral fraction was separated using magnetic and heavy liquid separation methods in

Table 2
LA-ICP-MS zircon U—Pb, in-situ Hf isotope analysis data.

	Content (ppm)				Isotopic ages (Ma)						Isotopic ratio				Model ages (Ma)	
	Pb	Th	U	Th/U	$^{207}Pb/^{206}Pb$	±1σ	$^{207}Pb/^{235}U$	±1σ	$^{206}Pb/^{238}U$	±1σ	$^{176}Lu/^{177}Hf$	$^{176}Hf/^{177}Hf$	±2σ	$\varepsilon_{Hf}(t)$	T_{DM1}	T_{DM2}
DN292																
1	3	108	74	1.46	302	148	162	9	155	3						
2	3	148	76	1.93	165	150	157	9	158	3						
3	3	86	83	1.03	72	156	154	11	161	4						
4	8	141	236	0.60	200	96	158	6	159	2						
5	10	188	282	0.67	206	74	166	5	163	2						
6	6	97	181	0.53	298	138	167	7	158	2						
7	2	64	73	0.87	165	−39	157	9	159	3						
8	38	536	1072	0.50	187	66	185	5	183	2						
9	4	81	111	0.73	317	115	171	8	160	3						
10	5	138	163	0.85	209	119	163	7	160	2						
11	11	164	326	0.50	298	86	192	7	183	3						
12	4	79	93	0.86	235	134	182	10	182	4						
13	11	253	335	0.76	167	85	158	6	159	2						
14	12	316	343	0.92	187	114	164	5	163	2						
15	5	193	136	1.42	300	133	169	9	161	2						
16	8	194	244	0.80	72	89	152	5	158	2						
17	7	274	163	1.68	406	111	175	7	159	2						
18	4	74	129	0.58	298	120	169	9	158	2						
19	7	121	201	0.60	372	96	173	7	159	2						
20	3	96	95	1.01	239	131	164	9	161	3						
DN117																
1	17	444	756	0.59	109	−97	112	5	111	2	0.001371	0.282688	0.000009	−0.6	806	1211
2	17	432	753	0.57	400	−300	107	4	111	2	0.001748	0.282605	0.000008	−3.6	935	1401
3	14	409	651	0.63	87	100	107	4	108	2	0.001651	0.282648	0.000008	−2.1	870	1305
4	19	556	812	0.68	198	324	111	15	108	2						
5	18	444	826	0.54	13	89	104	4	108	2						
6	14	314	644	0.49	100	94	110	5	110	2						
7	16	359	730	0.49	87	107	109	5	110	2	0.001542	0.282683	0.000009	−0.9	818	1226
8	14	343	639	0.54	54	113	108	5	110	2	0.001417	0.282617	0.000009	−3.2	909	1373
9	16	380	714	0.53	6	96	106	4	110	2	0.001638	0.282652	0.000009	−1.9	864	1294
10	24	752	1077	0.70	76	91	107	4	108	2						
11	16	380	733	0.52	122	93	111	4	110	2	0.001348	0.282669	0.000009	−1.3	833	1255
12	11	257	520	0.49	80	107	106	5	107	2						
13	16	399	705	0.57	78	106	117	6	118	2						
14	16	481	648	0.74	17	126	115	6	119	2						
15	15	356	716	0.50	122	98	108	4	108	2						
16	26	865	1137	0.76	65	78	108	4	110	2						
17	19	587	861	0.68	183	93	114	4	112	2						
18	16	463	690	0.67	167	93	111	4	109	2	0.001650	0.282630	0.000010	−2.7	896	1344
19	27	706	1225	0.58	172	81	115	4	112	2						
20	17	501	786	0.64	172	77	111	4	108	1						
DN138																
1	14	276	683	0.40	191	85	113	4	109	2						
2	16	341	763	0.45	122	91	108	4	108	1	0.001022	0.282647	0.000009	−2.1	858	1305
3	9	170	444	0.38	109	124	107	5	107	2	0.000703	0.282650	0.000009	−2.0	845	1296
4	16	392	778	0.50	132	99	109	4	108	2	0.001001	0.282689	0.000008	−0.6	798	1210
5	14	306	669	0.46	272	122	119	6	111	2						
6	13	312	619	0.51	309	122	119	5	110	2						
7	14	338	699	0.48	283	113	114	5	106	2						
8	14	282	700	0.40	54	93	105	4	107	2	0.001090	0.282655	0.000009	−1.9	847	1287
9	13	284	651	0.44	78	94	105	5	106	2						
10	15	338	748	0.45	187	102	110	5	106	2	0.000987	0.282689	0.000010	−0.7	798	1212
11	10	199	494	0.40	298	140	116	5	108	2						
12	13	330	640	0.52	217	135	113	7	106	2	0.000795	0.282712	0.000008	0.1	762	1159
13	16	399	805	0.50	122	−90	107	4	106	1	0.000834	0.282648	0.000008	−2.1	852	1303
14	11	233	543	0.43	50	93	103	4	105	2						
15	12	289	607	0.48	154	106	108	4	107	2	0.000974	0.282704	0.000008	−0.1	775	1176
16	13	294	618	0.48	80	119	107	5	108	2						
17	15	341	705	0.48	61	107	105	4	108	2						
18	13	294	627	0.47	256	119	112	6	105	2	0.000867	0.282681	0.000008	−1.0	806	1230
DN291																
1	15	379	733	0.52	76	100	105	4	106	2	0.000831	0.282675	0.000009	−1.2	814	1243
2	13	313	703	0.45	172	93	106	4	102	2	0.001595	0.282671	0.000009	−1.4	835	1255
3	14	325	677	0.48	191	94	110	4	106	2						
4	18	325	885	0.37	165	138	110	4	107	2	0.000900	0.282672	0.000009	−1.2	819	1248
5	17	379	785	0.48	98	111	116	6	116	2						
6	15	374	742	0.50	195	89	112	4	107	2						
7	14	348	691	0.50	124	119	105	5	105	2						

(continued on next page)

Table 2 (*continued*)

	Content (ppm)				Isotopic ages (Ma)						Isotopic ratio				Model ages (Ma)	
	Pb	Th	U	Th/U	$^{207}Pb/^{206}Pb$	±1σ	$^{207}Pb/^{235}U$	±1σ	$^{206}Pb/^{238}U$	±1σ	$^{176}Lu/^{177}Hf$	$^{176}Hf/^{177}Hf$	±2σ	$\varepsilon_{Hf}(t)$	T_{DM1}	T_{DM2}
8	12	255	614	0.42	128	117	106	5	105	2	0.000963	0.282660	0.000008	−1.7	838	1277
9	17	383	830	0.46	154	107	105	4	103	2						
10	14	252	680	0.37	191	108	109	4	106	2	0.000749	0.282660	0.000008	−1.7	833	1276
11	14	304	684	0.44	206	111	110	5	106	2	0.000787	0.282688	0.000010	−0.7	795	1213
12	24	426	1193	0.36	146	83	109	4	107	2						
13	12	308	633	0.49	298	140	109	5	102	3						
14	19	513	871	0.59	139	114	108	5	107	2	0.000770	0.282701	0.000009	−0.2	776	1183
15	16	284	818	0.35	195	104	106	4	102	2						
16	18	469	844	0.56	120	86	106	4	105	2	0.001127	0.282649	0.000009	−2.1	857	1303
17	23	541	1097	0.49	122	81	108	4	107	2						
18	9	177	427	0.41	209	112	111	5	106	2	0.001022	0.282617	0.000009	−3.2	900	1374
19	14	336	707	0.48	100	98	105	5	104	2						
20	14	337	687	0.49	200	118	108	4	107	2						
21	28	567	1411	0.40	100	94	107	5	107	2						
22	12	233	558	0.42	233	125	118	6	114	2						
23	17	371	885	0.42	106	104	105	4	105	1						
24	11	263	564	0.47	209	124	109	6	106	2	0.000897	0.282666	0.000008	−1.5	828	1263
DN259																
1	8	216	385	0.56	72	100	105	4	107	2						
2	9	264	416	0.63	176	89	109	4	106	1						
3	11	158	582	0.27	211	82	111	4	107	1						
4	7	144	340	0.42	176	127	110	4	107	1						
5	8	219	400	0.55	98	96	106	4	106	1						
6	7	284	294	0.96	233	96	108	4	103	1						
7	13	610	531	1.15	20	102	102	4	106	1						
8	9	262	417	0.63	122	93	105	4	104	1						
9	11	457	496	0.92	72	94	105	4	106	1						
10	11	171	348	0.49	33	83	155	5	163	2						
11	6	171	299	0.57	9	96	100	4	104	1						
12	6	153	284	0.54	76	107	104	5	105	1						
13	9	216	400	0.54	32	91	102	3	105	1						
14	9	322	386	0.83	132	107	108	5	106	2						
15	7	137	326	0.42	228	92	112	4	106	1						
16	13	234	638	0.37	139	89	106	4	105	1						
17	6	151	288	0.52	209	112	108	5	103	2						
18	7	188	333	0.57	65	107	104	5	106	2						
19	22	25	51	0.48	1787	52	1825	26	1849	22						
20	6	180	267	0.68	13	126	103	5	107	1						
DN196																
1	18	353	869	0.41	117	80	105	4	105	2	0.001241	0.282639	0.000008	−2.5	874	1326
2	15	312	748	0.42	139	106	107	5	104	2						
3	29	436	1466	0.30	39	100	102	4	105	2	0.001396	0.282646	0.000008	−2.2	867	1310
4	21	463	1088	0.43	400	−200	103	5	106	2						
5	12	257	627	0.41	100	113	103	4	104	2	0.000745	0.282672	0.000009	−1.3	815	1249
6	32	595	1688	0.35	35	87	102	3	104	2	0.001533	0.282661	0.000009	−1.8	849	1278
7	19	276	988	0.28	128	94	107	4	107	2						
8	17	368	833	0.44	154	106	106	4	104	1						
9	16	298	803	0.37	128	104	108	5	107	2	0.001328	0.282649	0.000008	−2.1	861	1301
10	11	202	540	0.37	109	118	108	5	109	2	0.001062	0.282644	0.000008	−2.2	862	1311
11	23	512	1164	0.44	195	75	109	4	105	2						
12	21	381	1022	0.37	306	78	115	4	106	2						
13	34	599	1735	0.35	198	70	108	3	105	2						
14	17	338	828	0.41	146	84	108	4	106	2						
15	13	241	632	0.38	76	96	105	4	106	2						
16	34	563	1734	0.32	117	68	102	3	101	1						
17	18	256	919	0.28	95	96	102	4	102	2						
18	18	298	857	0.35	20	102	101	4	104	2						
19	22	302	1069	0.28	124	89	106	4	104	2						
20	17	346	791	0.44	200	94	102	4	101	2	0.000934	0.282627	0.000008	−3.0	883	1353
21	20	259	965	0.27	132	99	105	4	104	2						
22	24	522	1197	0.44	6	93	99	4	104	2						
23	19	280	945	0.30	32	89	103	4	106	2						
24	21	381	1060	0.36	146	89	106	4	104	2	0.000893	0.282619	0.000010	−3.2	893	1369
DN040																
1	19	244	984	0.25	87	85	109	4	110	2						
2	28	463	1403	0.33	102	85	110	4	111	2						
3	18	244	946	0.26	61	104	104	4	106	2	0.001325	0.282687	0.000010	−0.8	807	1216
4	24	339	1244	0.27	189	123	113	4	110	2	0.001197	0.282659	0.000009	−1.7	844	1276
5	25	393	1296	0.30	50	96	106	4	108	2						
6	22	450	1076	0.42	233	55	112	4	107	2						
7	20	308	1035	0.30	95	117	105	4	106	2						

Table 2 (*continued*)

	Content (ppm)				Isotopic ages (Ma)						Isotopic ratio				Model ages (Ma)	
	Pb	Th	U	Th/U	$^{207}Pb/^{206}Pb$	±1σ	$^{207}Pb/^{235}U$	±1σ	$^{206}Pb/^{238}U$	±1σ	$^{176}Lu/^{177}Hf$	$^{176}Hf/^{177}Hf$	±2σ	$\varepsilon_{Hf}(t)$	T_{DM1}	T_{DM2}
8	26	406	1325	0.31	265	85	116	4	108	2						
9	29	438	1493	0.29	256	81	116	4	108	2	0.001029	0.282645	0.000008	−2.2	860	1308
10	27	465	1367	0.34	172	77	111	4	107	2	0.001314	0.282670	0.000008	−1.4	832	1256
11	25	375	1225	0.31	198	87	113	4	109	2	0.001297	0.282610	0.000009	−3.4	916	1388
12	22	289	1080	0.27	165	90	110	4	107	1						
13	19	401	865	0.46	139	94	112	4	111	2						
14	27	418	1314	0.32	32	74	103	3	106	1	0.001469	0.282662	0.000008	−1.7	846	1275
15	25	460	1201	0.38	65	85	106	4	107	1						
16	46	639	1785	0.36	206	36	137	4	132	2						
17	19	267	916	0.29	98	−105	107	4	107	2						
18	16	203	792	0.26	243	113	112	5	106	2	0.000951	0.282640	0.000007	−2.4	865	1321
19	29	422	1442	0.29	72	81	107	4	107	1	0.001285	0.282675	0.000010	−1.2	823	1242
20	23	467	1136	0.41	76	91	106	4	107	1						
DN054																
1	5	94	230	0.41	261	129	112	6	105	2						
2	8	161	408	0.39	117	100	106	4	105	1						
3	6	139	314	0.44	146	92	107	4	104	1						
4	7	146	319	0.46	302	114	116	6	106	2						
5	6	133	302	0.44	95	117	106	5	106	1						
6	11	168	484	0.35	17	104	112	5	115	2						
7	6	137	313	0.44	102	96	105	4	105	1						
8	6	114	292	0.39	124	108	106	4	105	1						
9	8	156	359	0.43	122	96	115	4	115	1						
10	6	145	290	0.50	76	93	105	4	106	1						
11	6	129	289	0.45	109	101	105	4	106	2						
12	6	157	271	0.58	183	94	109	5	106	2						
13	8	154	390	0.39	98	87	107	4	108	1						
14	8	182	378	0.48	209	90	109	4	105	1						
15	9	171	437	0.39	400	−298	103	4	107	1						
16	7	179	333	0.54	169	107	110	5	107	1						
17	6	153	304	0.50	167	98	109	4	106	1						
18	7	122	341	0.36	256	82	113	4	106	1						
19	6	142	283	0.50	83	93	105	4	105	1						
20	7	120	344	0.35	58	93	113	4	115	2						
21	6	156	288	0.54	65	124	104	5	106	2						
22	10	179	449	0.40	400	−313	112	4	116	2						
23	6	130	314	0.41	102	−103	106	4	105	1						
24	9	144	473	0.30	132	91	107	4	106	1						
DN090																
3	24	1805	921	1.96	76	74	96	3	97	1						
4	10	770	380	2.02	100	113	93	5	94	2						
5	8	565	329	1.72	100	120	95	5	96	2						
6	13	980	472	2.08	128	133	99	5	98	2						
7	5	333	215	1.55	232	152	103	7	98	2	0.001318	0.282518	0.000010	−6.9	1047	1602
8	18	1105	711	1.56	6	117	95	4	99	2						
9	6	449	259	1.73	76	144	94	5	96	2						
10	10	722	395	1.83	120	−84	101	4	100	2	0.001924	0.282536	0.000010	−6.3	1038	1562
11	6	407	243	1.68	132	141	99	6	98	2						
12	7	490	268	1.83	87	168	93	6	95	2	0.001277	0.282551	0.000009	−5.8	999	1529
13	7	525	285	1.84	183	145	100	6	98	2	0.001178	0.282522	0.000009	−6.8	1037	1592
14	14	472	526	0.90	117	80	122	4	123	2						
15	17	482	682	0.71	165	87	115	4	113	2						
16	19	1491	695	2.15	56	87	95	4	96	1						
17	15	1284	511	2.51	256	100	105	5	98	2	0.002081	0.282502	0.000014	−7.5	1092	1640
18	20	1459	799	1.83	58	96	95	4	96	1						
19	18	1067	746	1.43	317	80	106	4	96	1	0.001608	0.282547	0.000010	−5.9	1013	1538
DN178																
1	12	835	467	1.79	154	113	97	5	96	2	0.001884	0.282509	0.000011	−7.3	1076	1625
2	10	652	409	1.60	100	109	97	5	98	2	0.001749	0.282449	0.000009	−9.4	1158	1758
3	8	578	338	1.71	191	133	98	5	96	2						
4	13	266	596	0.45	122	80	107	3	108	2						
5	16	438	814	0.54	106	83	101	3	101	2	0.001061	0.282686	0.000009	−0.9	804	1222
6	12	772	491	1.57	235	66	104	4	99	2	0.001932	0.282531	0.000010	−6.5	1046	1575
7	12	807	464	1.74	232	102	105	4	100	2	0.001796	0.282529	0.000010	−6.5	1045	1578
8	11	688	472	1.46	239	93	102	4	97	2						
9	7	507	267	1.90	213	146	99	5	96	2	0.001575	0.282518	0.000010	−7.0	1054	1604
10	10	641	373	1.72	139	111	100	4	100	2	0.001103	0.282532	0.000010	−6.4	1021	1568
11	15	1420	535	2.66	257	108	101	4	95	2						
12	16	341	772	0.44	254	90	117	4	111	2						
13	23	1880	804	2.34	109	97	97	4	96	1						

(*continued on next page*)

Table 2 (*continued*)

	Content (ppm)				Isotopic ages (Ma)						Isotopic ratio				Model ages (Ma)	
	Pb	Th	U	Th/U	$^{207}Pb/^{206}Pb$	±1σ	$^{207}Pb/^{235}U$	±1σ	$^{206}Pb/^{238}U$	±1σ	$^{176}Lu/^{177}Hf$	$^{176}Hf/^{177}Hf$	±2σ	$\varepsilon_{Hf}(t)$	T_{DM1}	T_{DM2}
14	17	1101	663	1.66	200	95	102	4	100	2						
15	10	630	381	1.66	54	122	99	5	101	2						
16	9	580	357	1.63	333	119	107	5	99	2						
17	7	541	262	2.06	78	117	97	5	97	2	0.001107	0.282611	0.000011	−3.6	910	1392
18	22	1362	792	1.72	280	89	107	4	100	2	0.001781	0.282575	0.000010	−4.9	978	1474
19	9	620	338	1.83	167	126	99	5	97	2	0.001109	0.282574	0.000010	−4.9	962	1475
20	17	1529	540	2.83	146	106	101	4	98	2						
21	6	412	233	1.77	283	176	102	7	97	2						
22	31	2070	1013	2.04	328	89	122	5	111	2						
23	11	658	422	1.56	280	124	107	5	100	2						
24	13	880	499	1.76	211	103	103	4	99	2						
25	13	1024	476	2.15	467	119	108	5	96	2						

Notes: $\varepsilon_{Hf}(t) = 1000\{[(^{176}Hf/^{177}Hf)_S - (^{176}Lu/^{177}Hf)S \times (e^{\lambda t} - 1)] / [(^{176}Hf/^{177}Hf)_{CHUR,0} - (^{176}Lu/^{177}Hf)CHUR \times (e^{\lambda t} - 1)] - 1\}$.
$T_{DM1} = 1/\lambda \times \ln\{1 + [(^{176}Hf/^{177}Hf)_S - (^{176}Hf/^{177}Hf)_{DM}] / [((^{176}Lu/^{177}Hf)_S - (^{176}Lu/^{177}Hf)_{DM})]\}$.
$T_{DM2} = 1/\lambda \times \ln\{1 + [(^{176}Hf/^{177}Hf)_{S,t} - (^{176}Hf/^{177}Hf)_{DM,t}] / [((^{176}Lu/^{177}Hf)_c - (^{176}Lu/^{177}Hf)_{DM}]\} + t$.
The $^{176}Hf/^{177}Hf$ and $^{176}Lu/^{177}Hf$ ratios of chondrite and depleted mantle at the present day are 0.282772 and 0.0332, and 0.28325 and 0.0384, respectively (Griffin et al., 2004). $\lambda_{Lu} = 1.867 \times 10^{-11}$ year^{-1} (Soderlund et al., 2004). $(^{176}Lu/^{177}Hf)_C = 0.015$ (Griffin et al., 2002). It is the crystallization age of zircon.

order to concentrate zircons, which were then hand-picked under a binocular microscope. The morphology and internal structure of the zircons was studied via cathodoluminescence (CL) imaging using a JXA-8100 Electron Probe Microanalyzer with a Mono CL3 Cathodoluminescence System for high resolution imaging and spectroscopy at the Guangzhou Institute of Geochemistry, Chinese Academy of Sciences (GIGCAS).

LA-ICP-MS zircon U—Pb dating for all the samples was performed in the State Key Laboratory of Isotope Geochemistry, GIGCAS. Each analysis included a background acquisition of approximately 20–30 s followed by 50 s of data acquisition. NIST SRM 610 glass and Temora zircon standards were used as external standards. Each block of five unknowns was bracketed by analyses of standards. Off-line inspection and integration of background and analysis signals, and time-drift correction and quantitative calibration for trace element analyses and U—Pb dating were performed using ICPMSDataCal (Liu et al., 2008). Age calculation and plotting of concordia diagrams was performed using Isoplot Ex 3.0 (Ludwig, 2003). Detailed analytical techniques have been described by Yuan et al. (2004) and the analytical results are presented in Table 2.

Zircon Lu—Hf isotopic analyses were performed using a Nu Plasma HR MC-ICP-MS (Nu Instruments, UK), coupled to a 193 nm excimer laser ablation system (RESOlution M-50, Resonetics LLC, USA) in the State Key Laboratory of Isotope Geochemistry, GIGCAS. The measured isotopic ratios of $^{176}Hf/^{177}Hf$ were normalized to $^{179}Hf/^{177}Hf = 0.7325$, using exponential correction for mass bias. The measured in-situ $^{173}Yb/^{172}Yb$ ratio was used for mass bias correction for both Yb and Lu because of their similar physicochemical properties. Ratios used for the corrections were 0.5886 for $^{176}Yb/^{172}Yb$ (Chu et al., 2002) and 0.02655 for $^{176}Lu/^{175}Lu$ (Machado and Simonetti, 2001). The measured $^{176}Lu/^{177}Hf$ ratios and the ^{176}Lu decay constant of 1.867×10^{-11} year^{-1} reported by Soderlund et al. (2004) were used to calculate initial $^{176}Hf/^{177}Hf$ ratios. The chondritic values of $^{176}Hf/^{177}Hf = 0.0336$ and $^{176}Lu/^{177}Hf = 0.282785$ reported by Bouvier et al. (2008) were used for the calculation of $\varepsilon_{Hf}(t)$ values. The depleted mantle line is defined by present-day $^{176}Hf/^{177}Hf = 0.28325$ and $^{176}Lu/^{177}Hf = 0.0384$ (Griffin et al., 2004). Single-stage Hf model ages (T_{DM}) were calculated relative to the depleted mantle which is assumed to have linear isotopic growth from $^{176}Hf/^{177}Hf = 0.279718$ at 4.55Ga, to 0.283250 at present, with a $^{176}Lu/^{177}Hf = 0.0384$ (Griffin et al., 2004), and two-stage Hf model ages (T_{DM}) were calculated assuming a mean $^{76}Lu/^{177}Hf$ value of 0.015 for the average continental crust (Griffin et al., 2002). The analytical results are presented in Table 2.

4.2. Molybdenite Re—Os analytical method

Disseminated molybdenite crystals in the SOE were found in the hydrothermally altered Sifang granodiorite and Luoboling granodiorite porphyry with minor amounts in the quartz-dominated veins in the Wulongsi pluton. To constrain their formation ages, four molybdenite samples from three drill holes were selected for Re—Os analyses. Samples DN086 and DN209 are disseminated molybdenite in sericite altered granodiorite porphyry whereas DN101 and DN105 are molybdenite-bearing quartz veins in dickite and alunite altered granite.

Detailed molybdenite Re—Os analytical methods and results have been presented by Sun et al. (2010). Mineral separates were obtained by crushing the samples in a porcelain mill, gravity sorting, electromagnetic separation, and finally hand-picked under a binocular microscope (purity > 99%). Re—Os sample dissolution and preparation were performed at the Key Laboratory of Isotope Geochronology and Geochemistry, Guangzhou Institute of Geochemistry, Chinese Academy of Sciences. Re and Os concentration and isotopic composition were measured using a XSeries-2 quadrupole ICP-MS (Thermo Scientific, USA).

Table 3
Re—Os isotopic data.

Sample	Weight/g	Re/μg g^{-1}		^{187}Re/μg g^{-1}		^{187}Os/ng g^{-1}		Age/Ma	
		Content	2σ	Content	2σ	Content	2σ	Model T	2σ
DN101	0.016	327.635	1.6657	205.932	1.047	377.384	0.303	109.9	0.57
DN105	0.0149	345.037	1.6062	216.869	1.0096	389.974	0.7875	107.84	0.55
DN086	0.0038	2128.98	8.4576	1338.14	5.3159	2360.3	8.1253	105.78	0.56
DN209	0.0371	49.8754	0.2171	31.3486	0.1365	55.963	0.2796	107.06	0.71

Each sample was digested by the Carius tube method using concentrated HNO_3. In a Carius tube, ^{185}Re spike, natural Os standard solutions and molybdenite (0.004–0.04 g) were accurately weighed. The lower half of the tube was immersed in ethanol-liquid nitrogen slush. To this 10 ml concentrated HNO_3 was added. The sample-bearing tube was carefully for sealed and opened following the method described by Shirey and Walker (1995). The sealed tube was heated at 225–230 °C for 24 h. After sample digestion, the tube was refrozen, and then opened. Subsequently, an approximate amount of supernatant was transferred to a 30-ml quartz beaker, heated to dryness at 150 °C, and then 0.5 ml HNO_3 was added and dried down. This step was repeated twice to ensure removal of Os as OsO_4. The final solution was made up in 10 ml of 2% HNO_3 for ICP-MS determination of Re. The residual supernatant was poured into a 50-ml distillation flask redesigned after Sun et al. (2001, 2010) and distilled at 110 °C for 20 min followed by Os extraction with 5 ml of H_2O chilled in a water-ice bath. The H_2O solution was then used for ICP-MS determination of Os isotope ratio.

Average blanks for the whole procedure were ca. 2.8 pg for Re and 0.7 pg for Os, which was negligible for the measured Re and Os abundances. In order to eliminate memory effects of Os, the ICP-MS sampling system was flushed with 0.5% $H_2NNH_2 \cdot H_2O$ in 10% ethanol and 5% HNO_3 alternately, until the counts of ^{190}Os dropped to background level regardless of Os introduction. The Os water solutions were measured to obtain $^{187}Os/^{190}Os$ ratios for molybdenite. Results are presented in Table 3.

4.3. Whole-rock major and trace element analyses

The major and trace elements of the bulk rock samples were determined at the Mineral Division of ALS Chemex (Guangzhou) Co. Ltd. Whole rock samples were first powdered to <200 mesh, then fluxed with $Li_2B_4O_7$ and $LiBO_2$ to make homogeneous glass disks at 1050–1100 °C. The major elements were analyzed by X-ray fluorescence spectrometry on fused glass beads using a PANalytical Axios. The analytical precision for major elements was better than 1%. For trace element analyses, about 50 mg of powder for each sample was added to lithium metaborate flux, mixed well and fused in a furnace at 1000 °C. The resulting melt was then cooled and dissolved in 100 ml of 4% HNO_3 solution. The REE and trace element concentrations of the sample solutions were determined by inductively coupled plasma mass spectrometry (PerkinElmer Elan 9000) with the analytical precision better than 5% for most trace elements. The results of whole-rock major and trace elements analyses are listed in Table 4.

5. Results

5.1. Zircon U—Pb geochronology

The representative zircon CL images and analyzed spots with U—Pb ages and Lu—Hf isotope data for the eight samples are shown in Fig. 7. The analyzed zircons have a wide range of U and Th contents but the majority have high Th/U ratios (most > 0.4). Rare earth element patterns are typically characterized by HREE enrichment with positive Ce anomalies and negative Eu anomalies. Zircon grains are colorless, generally euhedral and predominantly prismatic, consistent with a magmatic origin (Belousova et al., 2002; Yang et al., 2014).

5.1.1. Caixi monzogranite (DN292)

Zircon crystals in the Caixi monzogranite are euhedral, ranging from 80 μm to 100 μm, with length to with ratios of 1:1 to 2:1 (Fig. 7a). Most grains are transparent and have dark zoning in the rims suggesting the interaction between the hydrothermal liquid and the magma in the late stage of the magmatic evolving process (Shu et al., 2013). They have Th/U ratios of 0.50 to 1.93. One zircon is distinct with a dark color (Fig. 7a) and a significantly higher $^{206}Pb/^{238}U$ age of 183 ± 2 Ma. Two zircon cores (Fig. 7a) yielded ages of 182 ± 4 Ma, 183 ± 3 Ma, and are interpreted as inherited zircons. The remaining seventeen zircons yielded a weighted mean age of 159.5 ± 1.1 Ma (1σ, MSWD = 0.81; Fig. 8a), which is interpreted to represent the crystallization age for the pluton.

5.1.2. Sifang granodiorite (DN117)

This sample has euhedral zircons that are 150 to 300 μm long and have length/width ratios between 2:1 and 3:1. Most grains have cores and narrow oscillatory zoning towards the rims, suggesting a magmatic origin (Fig. 7b). They have Th/U ratios of 0.49 to 0.76. Twenty analyses on 20 zircons yielded concordant $^{206}Pb/^{238}U$ dates ranging from 108 ± 2 Ma to 119 ± 2 Ma. Two zircons yielded significantly higher $^{206}Pb/^{238}U$ ages of 118 ± 2 Ma and 119 ± 2 Ma. These zircons are eroded and have oscillatory growth zones characteristic of a magmatic origin and are interpreted as inherited zircons. The remaining eighteen zircons yielded a weighted mean age of 109.5 ± 0.8 Ma (1σ, MSWD = 0.83; Fig. 8b), which is interpreted as the crystallization age for the pluton.

5.1.3. Shallow Luoboling granodiorite porphyry (P1, DN138)

This sample has euhedral zircons that are 100 to 200 μm long with length/width ratios between 1:1 and 3:1 (Fig. 7c). They have Th/U ratios of 0.38 to 0.52 and most of the grains have oscillatory growth zoning, suggestive of a magmatic origin. Eighteen analyses on 18 zircons yielded concordant $^{206}Pb/^{238}U$ ages ranging from 105 ± 2 Ma to 111 ± 2 Ma with a weighted mean age of 107.0 ± 0.8 Ma (1σ, MSWD = 0.80; Fig. 8c), interpreted to be the crystallization age for the pluton.

5.1.4. Deeper Luoboling granodiorite porphyry (P2, DN291)

This sample has euhedral zircons that are 100 to 300 μm long and have length/width ratios between 1:1 and 3:1 (Fig. 7d). They have Th/U ratios of 0.35 to 0.59. Twenty-four analyses on 24 zircons yielded concordant $^{206}Pb/^{238}U$ dates ranging from 102 ± 2 Ma to 116 ± 2 Ma. Two of these analyses show significantly higher $^{206}Pb/^{238}U$ ages of 114 ± 2 Ma, 116 ± 2 Ma and are interpreted as inherited zircons. The remaining twenty-two zircons yielded a weighted mean age of 105.4 ± 0.8 Ma (1σ, MSWD = 0.88; Fig. 8d) interpreted to be the crystallization age of the pluton.

5.1.5. Deepest Luoboling granodiorite porphyry (P3, DN259)

This sample has euhedral zircons that are 100 to 150 μm long and have length/width ratios between 1:1 and 2:1 (Fig. 7e). They have Th/U ratios of 0.27 to 1.15. Some of the grains have oscillatory growth zones and cores (Fig. 7e), suggestive of a magmatic origin. One zircon shows a distinct unzoned inner structure with a higher $^{206}Pb/^{238}U$ age of 1849 ± 22 Ma. Another inherited zircon core (Fig. 7e) yielded a $^{206}Pb/^{238}U$ age of 163 ± 2 Ma. The remaining eighteen zircons yielded a weighted mean age of 105.4 ± 0.62 Ma (1σ, MSWD = 0.70; Fig. 8e), which is interpreted to be the crystallization age for the pluton.

5.1.6. Dacite porphyry (D1 porphyry, DN040)

For this sample, the zircon crystals are euhedral, ranging from 100 μm to 250 μm in size, with length to width ratios of 2:1 to 3:1 (Fig. 7f). They have Th/U ratios of 0.25 to 0.46. All the grains have oscillatory growth zoning characteristic of a magmatic origin. Some grains have cores. One zircon with a distinct dark color (Fig. 7f) and subrounded shape yielded a significantly higher $^{206}Pb/^{238}U$ age of 132 ± 2 Ma. The remaining nineteen analyses yielded a weighted mean age of 107.5 ± 0.7 Ma (1σ, MSWD = 0.89; Fig. 8f) interpreted to be the crystallization age of the dacite.

5.1.7. Dacite porphyry (D2 porphyry, DN196)

This sample has euhedral zircons that are 150 μm to 250 μm long and have length/width ratios between 2:1 and 3:1 (Fig. 7g). They have Th/U ratios of 0.27 to 0.44. Most of the grains have oscillatory growth zonation suggestive of a magmatic origin. Twenty-four analyses on 24

Table 4
Major element (wt.%) and trace element (ppm) concentrations of the samples.

Rock	JM pluton			WL pluton	JL pluton	Caixi pluton			Sifang pluton						Dacite porphyry	
Types	ZJ10–13	ZJ10–14	ZJ10–15	DN101	ZJ10–26	SH-01	SH-02	SH-05	ZJ10–33	ZJ10–34	SH2–03	SH4–03	DN011	DN117	ZJ10–31	ZJ10–32
SiO_2	71.11	78.54	75.04	76.43	74.87	70.11	68.56	68.97	69.41	69.18	66.89	68.27	62.65	65.19	63.89	65.64
Al_2O_3	14.37	10.15	13.06	15.22	16.03	14.77	14.42	14.31	14.45	14.39	15.17	15.17	21.64	18.08	15.54	16.59
Fe_2O_3	2.57	0.85	0.73	0.93	0.86	3.11	3.81	3.63	2.98	3.25	3.95	3.47	4.4	7.12	3.09	1.87
FeO	0.9	0	0.35	0	0.2	0	0	0	1.3	1.55	0	0	0	0	1.6	0.7
MgO	0.39	0.16	0.16	0.11	0.15	0.79	1.07	1.01	1.15	1.3	1.68	1.34	0.11	0.09	1.21	0.7
CaO	0.51	0.32	0.24	0.04	0.07	2.36	2.86	2.68	3.21	3.22	3.97	3.67	0.18	0.11	3.48	2.51
Na_2O	4.38	0.18	3.96	0.06	0.06	2.91	3.13	2.95	3.25	2.75	2.97	3.06	0.14	0.12	2.29	2.48
K_2O	4.03	7.87	5.64	1.74	3	4.54	4.16	4.4	3.68	3.67	3.63	3.77	1.05	0.86	4.52	5.1
MnO	0.44	0.03	0.06	0.08	0.01	0.07	0.09	0.1	0.09	0.09	0.11	0.1	0.03	0.14	0.38	0.2
TiO_2	0.49	0.14	0.14	0.22	0.09	0.44	0.53	0.5	0.37	0.38	0.45	0.4	0.64	0.54	0.54	0.52
P_2O_5	0.13	0.04	0.04	0.06	0.08	0.13	0.17	0.17	0.16	0.18	0.19	0.17	0.29	0.22	0.21	0.22
LOI	1.32	1.32	0.69	4.3	4.65	0.9	0.67	0.84	0.99	1.36	1.01	0.52	8.58	7.45	4.53	3.89
Total	100.64	99.6	100.11	99.19	100.07	100.13	99.47	99.56	101.04	101.32	100.02	99.94	99.71	99.92	101.28	100.42
La	45.2	20	24.8	42.9	27.5	30.72	46.01	52.18	34.7	27.6	38.16	35.76	40.4	45.4	44.8	50.5
Ce	82.2	37.3	50.9	81.3	53.3	68.1	83.92	95.59	60.4	50.7	66.06	61.12	83.9	98.9	78.9	88.4
Pr	9.53	4.46	5.39	7.9	6.39	7.47	9.54	10.32	6.73	5.89	6.95	6.66	8.86	9.44	9.43	10.1
Nd	32.9	17	20.7	25.6	23.4	28.77	33.44	36.14	24.9	22.5	23.99	23.47	32.5	34.3	35.2	36.5
Sm	6.41	3.75	4.9	3.97	5.47	5.64	6.78	6.94	4.16	4.15	4.52	4.47	6.77	5.74	5.33	5.74
Eu	1.1	0.63	0.83	0.39	0.55	1.06	1.13	1.22	1.3	1.38	1.04	1.13	1.31	1.25	1.42	1.67
Gd	5.16	3.74	4.68	2.72	4.64	5.27	5.98	5.93	3.53	3.58	3.58	3.71	4.62	4.37	4.21	4.05
Tb	0.89	0.73	0.91	0.54	0.96	0.86	0.91	0.87	0.6	0.58	0.51	0.54	0.63	0.67	0.53	0.52
Dy	5.11	4.36	5.19	3.48	5.72	5.41	5.35	5.09	3.02	2.95	2.91	2.96	3.53	3.68	2.28	2.25
Ho	0.97	0.92	1.09	0.88	1.22	1.05	1.13	1.04	0.66	0.6	0.61	0.62	0.78	0.77	0.39	0.37
Er	2.84	2.83	3.03	2.75	3.26	3.13	3.22	2.96	1.82	1.66	1.79	1.84	2.14	2.08	1.17	1
Tm	0.49	0.49	0.61	0.53	0.61	0.48	0.55	0.52	0.31	0.27	0.3	0.31	0.39	0.32	0.16	0.14
Yb	3.21	3.25	3.83	3.88	3.85	2.97	3.7	3.19	2.12	1.82	2.01	2.07	2.58	2.49	0.99	0.87
Lu	0.47	0.47	0.57	0.55	0.67	0.45	0.55	0.47	0.33	0.29	0.32	0.31	0.38	0.37	0.14	0.12
Ta	4.81	3.79	5.53	2.61	8.55	1.95	1.95	1.84	1.02	1.33	1.35	1.31	0.6	0.51	1.05	0.98
Pb	39.9	82.1	47.5	100	860	17.9	27.34	33.31	15	14	13.81	14.16	153	81.3	23.4	280
Th	26.9	27.1	23.7	28.9	32.6	15.28	21.34	20.07	13.5	14	16.04	15.35	27.2	18	15.7	16.6
U	8.58	13.4	11.8	6.3	22.4	3.78	5.66	4.85	3.04	4.51	5.1	4.36	6.46	2.75	3.7	3.34
Zr	107	90.6	88.8	44.8	104	205	225	216	73.4	78.9	122	130	55.3	27.6	73	90.8
Hf	3.56	3.57	4.22	1.8	4.22	5.44	6.11	5.76	2.19	2.59	3.43	3.52	1.7	1	2.43	2.77
Ba	558	850	484	91.8	152	498.32	439.32	582.69	982	831	644.8	761.25	603	469	995	951
Rb	197	377	248	78.4	182	106.7	201.1	231.2	128	136	135.1	130.9	37.1	29.3	193	189
Sr	148	64.6	82.6	123.5	121	202.2	270.16	271.8	345	385	473.2	433.3	464	294	310	251
Y	28.3	26.5	32	5.9	37.5	27.21	30.29	27.15	18.2	16.4	15.59	16.76	11.8	10.2	11.5	10.4
Nb	26.4	19.8	22.4	15	44.1	18.5	21.54	19.57	14.2	14.4	13.36	14.13	6.7	6.4	12.5	12.1
REE	196.47	99.92	127.43	177.39	137.53	161.38	202.21	222.46	144.57	123.97	152.74	144.97	188.79	209.78	184.95	202.24
LREE	177.34	83.14	107.52	162.06	116.61	141.76	180.81	202.39	132.19	112.22	140.71	132.61	173.74	195.03	175.08	192.91
HREE	19.13	16.78	19.91	15.33	20.92	19.62	21.4	20.07	12.38	11.75	12.02	12.36	15.05	14.75	9.87	9.33
$(La/Yb)_N$	9.49	4.15	4.37	7.45	4.82	6.97	8.37	11.03	11.04	10.22	12.82	11.65	10.56	12.29	30.66	38.96
				$(Tb/Yb)_N$	1.22	0.99	1.04	0.61	1.09	1.28	1.08	1.21	1.25	1.39	1.11	1.16
1.21	1.36	2.02	1.47													
Eu/Eu*	0.19	0.17	0.17	0.12	0.11	0.19	0.18	0.19	0.34	0.36	0.26	0.28	0.23	0.25	0.30	0.34

Notes:
JM pluton refers to Jingmei pluton.
WL pluton refers to Wulongsi pluton.
JL pluton refers to Jinlongqiao pluton.
The dates abbreviate with "ZJ" from Jiang et al. (2013).
The dates abbreviate with "SH" and "ZK" from Zhao et al. (2007).
The dates abbreviate with "EMG" from Li et al. (2013b).

zircons yielded concordant $^{206}Pb/^{238}U$ dates ranging from 101 ± 1 Ma to 108.6 ± 2 Ma, giving a weighted mean age of 104.5 ± 0.7 Ma (1σ, MSWD = 0.96; Fig. 8g), interpreted to represent the crystallization age of the sample.

5.1.8. Quartz diorite porphyry (DN054)

Theses sample have euhedral zircons that are 150 μm to 300 μm long with length/width ratios between 1:1 and 3:1 (Fig. 7h). They have Th/U ratios of 0.30 to 0.58. Most of the grains have oscillatory growth zonation in the rim and cores, suggestive of a magmatic origin. Four zircon cores (Fig. 7h) yielded higher $^{206}Pb/^{238}U$ ages of 115 ± 2 Ma, 115 ± 1 Ma, 115 ± 2 Ma, 116 ± 2 Ma, and are interpreted to be inherited crystals. The remaining twenty zircons yielded a weighted mean age of 105.7 ± 0.61 Ma (1σ, MSWD = 0.47; Fig. 8h), interpreted to be the crystallization age of the pluton.

5.1.9. Rhyodacite (DN178)

This sample has subhedral to euhedral zircons that are 100 to 200 μm long with length/width ratios between 1:1 and 2:1 (Fig. 7i). They have relatively high Th/U ratios of 1.71 to 2.15. Some of the grains have oscillatory growth zonation and typical sector zoning, suggestive of a magmatic origin. Twenty-five analyses yielded concordant $^{206}Pb/^{238}U$ dates ranging from 96.3 ± 2 Ma to 111 ± 2 Ma. Three of these analyses show significantly higher $^{206}Pb/^{238}U$ ages of 108 ± 2 Ma, 111 ± 2 Ma, 111 ± 2 Ma, respectively, which are interpreted as ages for the inherited zircons. The remaining twenty-two zircons yielded a weighted mean age of 98.0 ± 0.8 Ma (1σ, MSWD = 1.03; Fig. 8i), representing the crystallization age of the sample.

5.1.10. Rhyolite (DN090)

This sample has subhedral to euhedral zircons that are 50 μm to 100 μm long with length/width ratios between 1:1 and 2:1 (Fig. 7j). They have relatively high Th/U ratios of 1.43 to 2.51. Most of the grains have oscillatory growth zonation and sector zoning, suggestive of a magmatic origin. Nineteen analyses yielded concordant $^{206}Pb/^{238}U$ dates ranging from 94 ± 1 Ma to 101 ± 2 Ma. One zircon core (Fig. 7j) yielded an older $^{206}Pb/^{238}U$ age of 123 ± 2 Ma whereas a second yielded a $^{206}Pb/^{238}U$ age of 113 ± 2 Ma (Fig. 7j), both of which are

Dacite porphyry					Luoboling pluton					Rhyolite	Rhyodacite	Quartz diorite porphyry
EMG-1	EMG-2	DN040	DN114	DN196	ZK402–1	ZK402–2	ZK402–4	DN291	DN138	DN090	DN178	DN054
67.54	67.8	64.45	69.86	64.48	64.94	64.65	65.01	62.42	63.24	69.11	67.59	60.62
16.29	16.03	16.62	18.64	16.5	15.25	15.19	15.08	15.42	15.51	15.31	15.18	15.73
2.77	2.54	6.88	1.46	5.57	3.84	4.59	4.56	5.59	4.83	3.25	8.17	7.06
0	0	0	0	0	0	0	0	0	0	0	0	0
0.73	0.33	0.19	0.19	1.28	1.9	2.06	2.13	1.95	1.9	0.86	0.1	2.86
3.52	3.24	0.33	0.25	0.04	3.17	3.98	3.85	3.19	2.82	0.57	0.13	1.44
2.79	2.63	0.14	0.15	0.3	3.02	3	2.98	2.85	2.8	1.08	0.1	3.62
4.02	4.27	1.58	2.3	4.47	3.21	3.54	4.01	3.7	4.34	5.66	0.61	3.83
0.2	0.03	0.07	0.03	0.08	0.05	0.12	0.1	0.1	0.13	0.08	0.05	0.29
0.52	0.56	0.84	0.95	0.61	0.46	0.53	0.54	0.52	0.45	0.37	0.49	0.59
0.22	0.3	0.45	0.42	0.2	0.22	0.24	0.24	0.25	0.23	0.11	0.18	0.28
0.89	2.44	8.54	4.99	5.51	2.62	1.49	1.18	2.12	2.86	2.82	7.46	2.69
99.49	100.17	100.09	99.24	99.04	98.68	99.39	99.68	98.11	99.11	99.22	100.06	99.01
34.81	30.15	51.5	46.7	29.6	36.19	38.01	34.23	38.8	39.4	93.3	30.1	35.7
78.5	62.18	79.6	106	67.9	61.57	67.61	62.33	64.3	58.5	200	49.7	69.3
7.61	6.63	10.8	9.66	6.47	6.69	7.79	6.87	7.53	7.05	17.1	4.32	6.93
20.31	26.03	41.1	36.5	25	22.19	25.98	23.66	27.3	24.6	60.3	14.7	26.1
5.34	5.59	6.59	6.58	4.65	4.25	5.55	4.98	4.84	4.16	9.77	2.45	5.03
1.42	1.15	1.59	1.68	1.17	0.94	1.04	1.03	1.06	0.92	1.81	0.66	1.27
3.37	4.08	4.54	5.07	4.13	3.77	4.25	3.78	3.23	2.72	6.56	2.01	3.72
0.53	0.55	0.59	0.91	0.68	0.52	0.64	0.55	0.51	0.42	0.86	0.31	0.56
2.28	2.9	2.72	4.65	4.75	2.8	3.44	2.99	2.66	2.51	4.14	1.59	2.9
0.53	0.6	0.57	0.94	1.25	0.55	0.75	0.62	0.58	0.48	0.84	0.31	0.69
1.65	1.84	1.62	2.31	4.02	1.64	2.08	1.79	1.55	1.44	1.93	0.78	1.66
0.22	0.3	0.25	0.34	0.56	0.29	0.35	0.31	0.26	0.24	0.32	0.13	0.25
1.77	1.97	1.83	2.41	2.75	1.79	2.24	2.04	1.64	1.53	1.88	0.93	1.81
0.28	0.34	0.3	0.33	0.36	0.28	0.33	0.31	0.27	0.26	0.3	0.17	0.26
2.18	2.26	1.01	1.43	1.13	1.63	1.62	2.32	1.55	1.53	1.71	0.19	1.33
277	1411	190.5	80.6	585	20.22	17.35	18.34	52.6	18.6	20.6	14	26.9
15.78	16.36	13.2	21.7	16.65	20.81	19.76	22.71	22.2	23.3	29.3	25.1	19.15
7.56	8.02	4.86	5.91	5.96	7.9	5.85	8.87	8.33	8.31	5.3	2.72	7.1
127	136	207	113	77.2	152	179	158	31.6	33.1	202	22.3	71.7
3.19	3.86	5.1	3.1	2.4	4.07	4.65	4.29	1.2	1.2	5.4	0.8	2
135	167	386	728	624	638.01	738.22	765.17	693	808	1320	274	910
193	245	69.4	120	229	119.7	136.3	158.6	138	172	221	24.9	132
1391	1297	299	269	22.8	510.8	529	506.8	501	425	119.5	112	291
11.51	14.2	13.5	19.1	35.8	15.12	19.26	16.89	11.8	11.2	22.5	7	15.1
19.44	20.08	17.2	16.3	12.1	14.89	15.48	18.32	14	13.9	21.7	2	13.7
158.62	144.31	203.6	224.08	153.29	143.45	160.05	145.47	154.53	144.23	399.11	108.16	156.18
147.99	131.73	191.18	207.12	134.79	131.83	145.98	133.1	143.83	134.63	382.28	101.93	144.33
10.63	12.58	12.42	16.96	18.5	11.63	14.08	12.37	10.7	9.6	16.83	6.23	11.85
13.26	10.32	18.97	13.06	7.26	13.65	11.45	11.34	15.95	17.36	13.30	33.46	21.82
1.32	1.23	1.42	1.66	1.09	1.29	1.25	1.18	1.37	1.21	1.36	2.02	1.47
0.33	0.24	0.29	0.29	0.27	0.23	0.21	0.24	0.26	0.27	0.22	0.30	0.29

interpreted as inherited zircons. The remaining zircons yielded a weighted mean age of 97.3 ± 0.8 Ma (1σ, MSWD = 0.57; Fig. 8j), which is interpreted the age of the rhyolite.

5.2. Zircon in-situ Lu—Hf isotopes

Zircon Lu—Hf isotopes were determined for 59 points from eight samples on the same or similar domains of the zircon grains dated for this study (inherited zircons not included). The analytical results are listed in Table 2.

Eight spots were analyzed on zircon grains from the Sifang granodiorite (DN117), yielding $\varepsilon_{Hf}(t)$ values from −3.6 to −0.6 with an average value of −2.0 and calculated T_{DM2} ages ranging from 1.40 Ga to 1.21 Ga. Nine spots from the P1 porphyry (DN138) yielded $\varepsilon_{Hf}(t)$ values from −2.1 to 0.1 with an average value of −1.2 and calculated T_{DM2} ages ranging from 1.31 Ga to 1.16 Ga. Ten spots from the P2 porphyry (DN291) yielded $\varepsilon_{Hf}(t)$ values from −3.2 to −0.2 with an average value of −1.5 and calculated T_{DM2} ages ranging from 1.37 Ga to 1.18 Ga. Eight spots from the D1 dacite porphyry (DN196) yielded $\varepsilon_{Hf}(t)$ values from −3.2 to −1.3 with an average value of −2.3 and calculated T_{DM2} ages ranging from 1.37 Ga to 1.25 Ga. Eight spots from the D2 dacite porphyry (DN040) yielded $\varepsilon_{Hf}(t)$ values from −3.4 to −0.8 with an average value of −1.8 and calculated T_{DM2} ages ranging from 1.39 Ga to 1.22 Ga. Six spots from the rhyolite (DN090) yielded $\varepsilon_{Hf}(t)$ values from −7.5 to −5.8 with an average value of −6.5 and calculated T_{DM2} ages ranging from 1.64 Ga to 1.53 Ga. Ten spots from the rhyodacite (DN178) yielded $\varepsilon_{Hf}(t)$ values from −9.4 to −0.9 with an average value of −5.7 and calculated T_{DM2} ages ranging from 1.76 Ga to 1.22 Ga. The $\varepsilon_{Hf}(t)$ values for Jingmei pluton, Wulongsi pluton and Jinlongqiao pluton are −9.7 ~ −7.1, −11.9 ~ −7.7 and −13.9 ~ −8.1, respectively (Li et al., 2015). The calculated T_{DM2} ages for Jingmei pluton, Wulongsi pluton and Jinlongqiao pluton are 1.8 Ga–1.62 Ga, 1.93 Ga–1.67 Ga and 2.05 Ga–1.69 Ga, respectively (Li et al., 2015).

5.3. Molybdenite Re—Os ages

Total ^{187}Re and ^{187}Os concentrations in all samples vary from 31 to 1338 μg and 55 to 2360 ng, respectively. The high radiogenic ^{187}Os values indicate that the content of common Os can be ignored when calculating the Re—Os model age. The molybdenite from two molybdenite-bearing quartz veins (DN101 and DN105) yielded model ages of 109.9 ± 0.57 Ma and 107.8 ± 0.55 Ma whereas the two disseminated molybdenite samples (DN209 and DN086) yielded model ages of 107.0 ± 0.71 Ma and 105.7 ± 0.56 Ma (Table 3). The four samples yielded a ^{187}Re—^{187}Os isochron age of 105.5 ± 2.2 Ma (2σ, MSWD = 56; Fig. 9b) and a weighted average age of 107.7 ± 2.8 Ma (2σ,

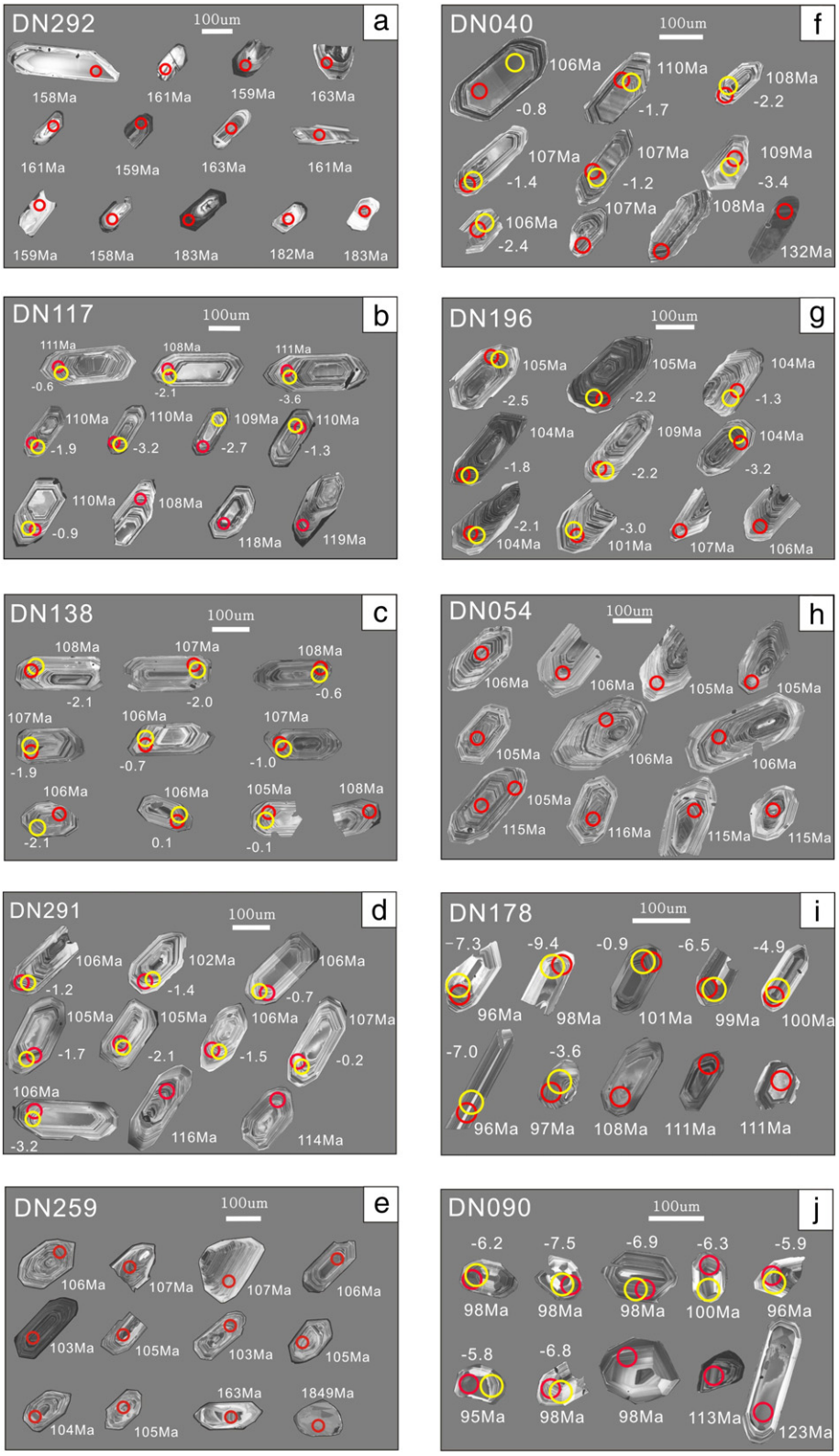

Fig. 7. Representative zircon CL images and analyzed spots with U—Pb ages and Lu—Hf isotope data.

MSWD = 37; Fig. 9a). The analytical errors of the samples are small which may explain the high deviations between the samples and the calculated regression line, and the high MSWD values (Wendt and Carl, 1991) but would not affect the reliability of the ^{187}Re—^{187}Os isochron age as the four samples are located almost on the same regression line (Fig. 9b).

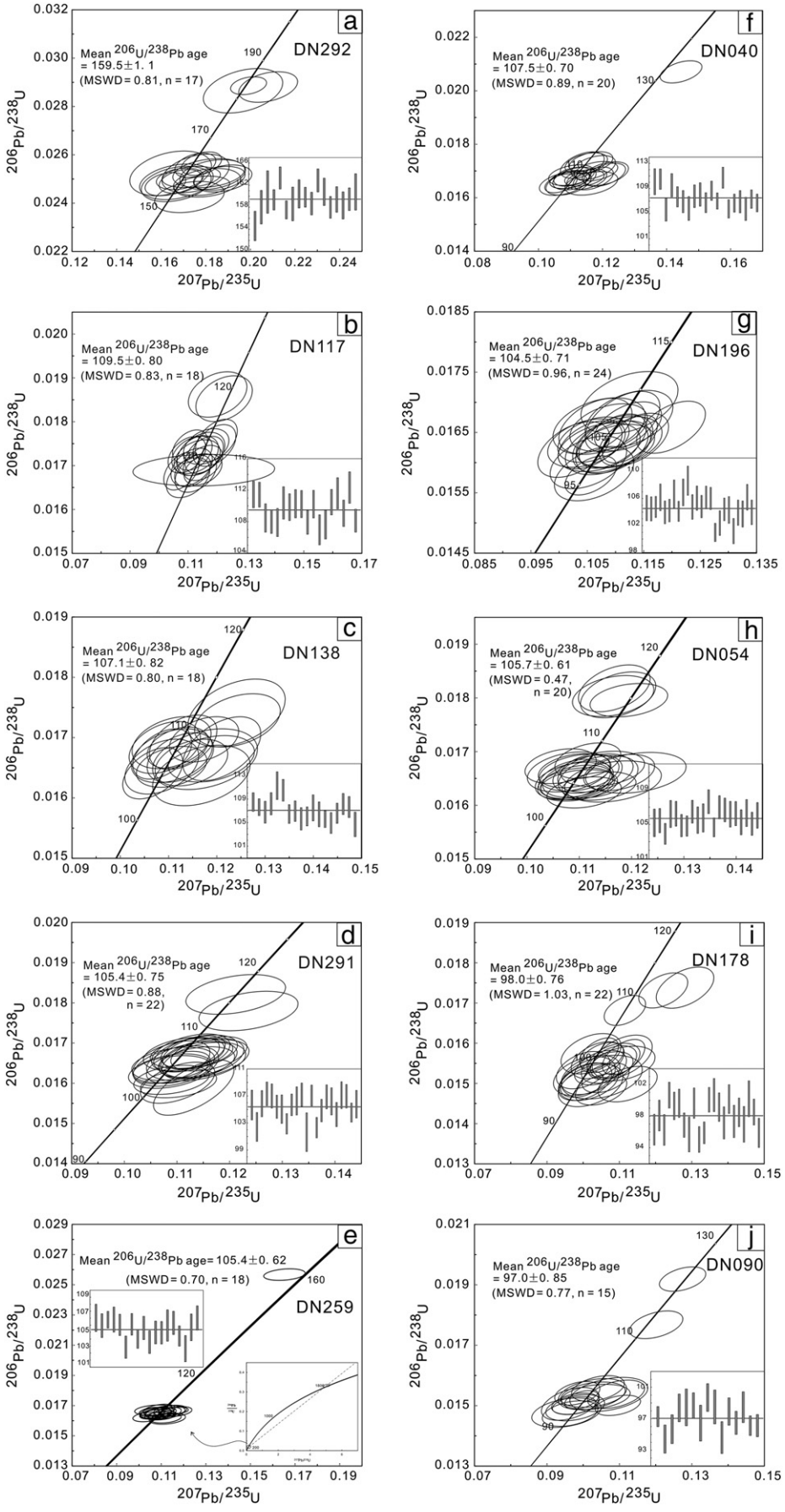

Fig. 8. Concordia plots and age data bar charts for zircon LA–ICP-MS U—Pb data from the intrusions and volcanic rocks in the Southeast Ore Segment.

5.4. Major and trace element contents

Eleven samples were analyzed for their major and trace element contents. Since the Zijinshan granite complex and the Caixi monzogranite have already been well-studied with abundant published data, in this study we focused on the Cretaceous igneous rocks from the SOE (except for one sample from the Jurassic Wulongsi pluton). These samples have variable LOI reflecting $H_2O + CO_2$ contents, due to different degrees of alteration. Major and trace element data for the Late Cretaceous plutons and volcanic rocks are listed in Table 4.

The Sifang granodiorite has been intensely altered (LOI > 7%), with low Na_2O-K_2O-CaO contents (totaling < 2%). The Wulongsi pluton, the dacite porphyry and the rhyodacite in the SOE have also been altered (LOI > 4%). Since many of the major elements (i.e., Ca, Na, P, K and Mg) are highly mobile during hydrothermal alteration (Middelburg et al., 1988), the alteration box plot of Large et al. (2001) was used to test this. Almost all of the rocks (except the Luoboling pluton and the quartz diorite porphyry) lie outside the field of least altered rocks and trend towards the fields of sericite, chlorite and pyrite alteration (Fig. 10a), consistent with the petrographic observations. Since the samples are intensively altered, the TAS diagram cannot be used for classification.

On a plot of SiO_2 vs. Zr/TiO_2 (Fig. 10b; Winchester and Floyd, 1977), the Zijinshan granite complex and Caixi pluton (with data from Jiang et al., 2013; Zhao, 2007) plot in the granite and granodiorite field; the Sifang pluton samples (with data from Jiang et al., 2013; Zhao, 2007) plot in the granodiorite field; the Luoboling pluton samples (with data from Zhao, 2007) plot in the granodiorite and diorite field; the dacite porphyry samples (with data from Li et al., 2013b; Jiang et al., 2013) plot in the rhyodacite/dacite field; whereas the quartz diorite porphyry plots in the diorite field, and the rhyolite and the rhyodacite (identified in the field) samples fall in the rhyodacite/dacite field. Further, the studied rocks show shoshonitic character (Fig. 10c).

On primitive mantle-normalized multi-element plots (Fig. 11a), the samples show characteristics of arc-related magmas (Pearce and Peate, 1995; Villagómez et al., 2011) with large-ion lithophile element (LILEs; e.g., Rb, K and Pb) enrichment and high field strength element (HFSEs; e.g., Nb, Ta, and Ti) depletions. The Middle to Late Jurassic Zijinshan granite complex and Caixi monzogranite display consistent REE patterns, characterized by LREE enrichment, flat HREE ($(La/Yb)_N = 4.15–11.03$; $(Tb/Yb)_N = 0.61–1.28$; Fig. 11b; Table 4) and moderate negative Eu anomalies ($Eu/Eu^* = 0.11–0.19$; Fig. 11b; Table 4).

The late Early Cretaceous samples (including the Sifang pluton, the Luoboling pluton, the dacite porphyry and the quartz diorite porphyry) are also characteristic of arc-related magmas, with LILE enrichment but stronger HFSE depletions than the Middle to Late Jurassic rocks and the early Late Cretaceous rocks (Fig. 11c). Chondrite normalized REE patterns for the late Early Cretaceous rocks are enriched in LREE relative to HREE, with the $(La/Yb)_N = 7.26–38.96$; $(Tb/Yb)_N = 1.08–2.63$, and weak Eu anomalies ($Eu/Eu^* = 0.21–0.36$) (Fig. 11d; Table 4).

All the early Late Cretaceous samples (the rhyolite and the rhyodacite) are enriched in Ba, Th, U and depleted in Nb, Ta, Zr, Hf (Fig. 11e). Compared with the rhyodacite, the rhyolite has an obvious Ti depletion. Chondrite normalized REE patterns for the late Early Cretaceous rocks are enriched in LREE relative to HREE, with the $(La/Yb)_N = 21.82–33.46$; $(Tb/Yb)_N = 1.47–2.02$, and weak Eu anomalies ($Eu/Eu^* = 0.22–0.30$) (Fig. 11f; Table 4).

5.5. Oxygen fugacity

The zircon Ce^{IV}/Ce^{III} ratios can be used as measures of the oxidation state of the magma (Ballard et al., 2002; Liang et al., 2006). The calculated results for eight samples are listed in Table 5. The Ce^{IV}/Ce^{III} ratios for the Sifang pluton range from 622 to 1236, 143 to 855 for the P1 porphyry, 277 to 1039 for P2 porphyry, 118 to 1800 for the D1 porphyry, 267 to 1627 for the D2 porphyry and 113 to 1021 for the quartz diorite porphyry. The early Late Cretaceous rocks (rhyodacite and the rhyolite) generally have lower Ce^{IV}/Ce^{III} ratios. The Ce^{IV}/Ce^{III} ratios for the rhyodacite range from 9 to 377 whereas ratios for the rhyolite range from 26 to 545

The Sifang granodiorite has Eu_N/Eu_N^* ranging from 0.5 to 0.7 and Ce_N/Ce_N^* of 44 to 1148. Zircon grains from the P1 porphyry display Ce anomalies ranging from 1 to 758 and Eu anomalies of 0.4–0.7 whereas the zircons in the P2 porphyry show Eu_N/Eu_N^* values of 0.4–0.6 and Ce_N/Ce_N^* of 2–659. Zircon grains from D1 porphyry display Ce anomalies ranging from 2 to 621 and Eu anomalies of 0.5–0.7 whereas the grains in the D2 porphyry have an Eu_N/Eu_N^* range of 0.5–0.7 and Ce_N/Ce_N^* range of 4–764. Zircon grains from rhyodacite display Ce anomalies ranging from 4 to 662 and Eu anomalies of 0.4–0.6 whereas the grains in the rhyolite show a Eu_N/Eu_N^* range of 0.4–0.5 and Ce_N/Ce_N^* range of 10–915.

6. Discussion

6.1. Timing of the magmatic sequences and mineralization in SOE and Zijinshan mineral field

Previous work has shown that there are two distinct magmatic events in the Zijinshan mineral field, i.e., the Middle to Late Jurassic and the Cretaceous (Jiang et al., 2013). Data from this study shows that the Cretaceous event can be further divided into two events. Therefore the magmatic events in the SOE can be divided into the Middle to Late Jurassic (165–150 Ma), late Early Cretaceous (110–105 Ma), and early Late Cretaceous (100–95 Ma) magmatic activity.

Rb—Sr ages for the Jingmei and Wulongsi plutons of 157 ± 7.3 Ma and 141 ± 6.7 Ma (Zhang et al., 2001), should be treated with caution due to intensive alteration and mobility of the LILE. Jiang et al. (2013) reported LA-ICP-MS zircon U—Pb ages for the Jingmei, Wulongsi and Jinlongqiao plutons of 165 ± 1 Ma, 164 ± 0.5 Ma, 157 ± 1 Ma, respectively. Li et al. (2015) reported almost the same age for the Zijinshan granite complex. In this study, we have found a ca. 163 Ma inherited zircon in P3, similar to that of the Zijinshan granite complex. All of which suggest the Zijinshan granite complex was emplaced between 165 Ma to 155 Ma.

Zhao et al. (2007) reported a SHRIMP zircon age of 150 ± 3 Ma for the Caixi monzogranite. This study yielded a $^{206}Pb/^{238}U$ age of 159.5 ± 1.1 Ma for an altered portion of the Caixi monzogranite. Hence, we propose that the Caixi monzogranite at Zijinshan formed between 160 to 150 Ma. Three older inherited zircons found in the Caixi pluton with an average age of ca. 183 Ma, suggesting a weak Early Jurassic magmatism in the Zijinshan district, similar to the Jurassic magmatic event (180–150 Ma) in the south of Nanling Belt close to the Zijinshan district (Hua et al., 2005).

Zhang et al. (2001) reported an approximate whole rock Rb—Sr isochron age of 128 ± 9 Ma for the Sifang granodiorite whereas Jiang et al. (2013) presented a LA-ICP-MS zircon U—Pb age of 112 ± 0.5 Ma which is consistent with the 110 ± 0.7 Ma reported here. This is interpreted to represent the beginning of Early Cretaceous magmatic activity in the SOE and the Zijinshan mineral field. In this study, we have found three inherited zircon grains from the rhyodacite yielding an age of ca. 110 Ma (ranging from ca. 111 Ma to 108 Ma), broadly coeval with the Sifang pluton. Two inherited zircons from the Sifang pluton yielded ages of 119 Ma and 118 Ma, which do not match any magmatic event found in Zijinshan district. According to Wang and Lu (1997), the collision event between the Fujian-Taiwan microcontinent and the Zhejiang Mesozoic volcanic arc took place from 120 Ma to 100 Ma. Thus the inherited zircons with an age of ca. 120 Ma may be linked to that event.

As for the Luoboling granodiorite porphyry, the weighted mean $^{206}Pb/^{238}U$ ages for the P1, P2 and P3 porphyries are 107 ± 0.7 Ma, 105 ± 0.7 Ma, 105 ± 0.6 Ma, respectively. The 107.5 ± 0.7 Ma and

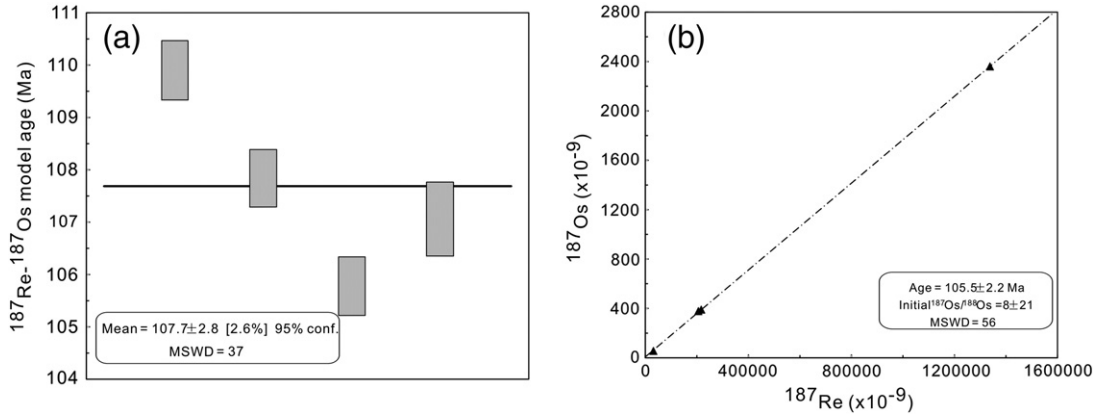

Fig. 9. Re—Os weighted mean model age diagram (a) and Re—Os isotopic isochron diagram (b) of molybdenite separated from the Southeast Ore Segment.

104.5 ± 0.7 Ma ages of the dacite porphyries are within error of the P1 and P2 and/or P3 porphyries. Two inherited zircons from the P2 porphyry from the quartz diorite porphyry yield an average age of ca. 115 Ma (ranging from 114 Ma to 116 Ma), suggesting a small magmatism in the Zijinshan district, that may be related to the collision event (120–100 Ma) between the Fujian-Taiwan microcontinent and the Zhejiang Mesozoic volcanic arc. Further, four inherited zircons from the quartz diorite porphyry yield an average age of ca. 115 Ma (ranging from 115 Ma to 116 Ma), may also be related to the collision event. The inherited zircon from the D1 porphyry has an age of ca. 132 Ma which may be indicative of a small magmatic event in the Zijinshan district generally consistent with the second episode (129–122 Ma) of Cretaceous magmatism in southeast China (Li, 2000). The molybdenite Re—Os ages show that the porphyry Cu mineralization in the SOE and Zijinshan district occurred between 110 Ma to 105 Ma, coeval with the emplacement age of the Sifang granodiorite, the Luoboling granodiorite porphyry, dacite porphyry and the quartz diorite porphyry.

The ~98 Ma rhyodacite and ~97 Ma rhyolite in the SOE are clearly post-mineralization and broadly coeval with the 95.9 ± 0.6 Ma unmineralized Zhongliao porphyritic biotite-granodiorite in the Luoboling area of the Zijinshan mineral field (Li and Jiang, 2014a). Inherited zircons from the rhyolite yielded ages of ca. 123 Ma and ca. 113 Ma, which may relate to the beginning and peak age of the collision event between the Fujian-Taiwan microcontinent and the Zhejiang Mesozoic volcanic arc (120–100 Ma).

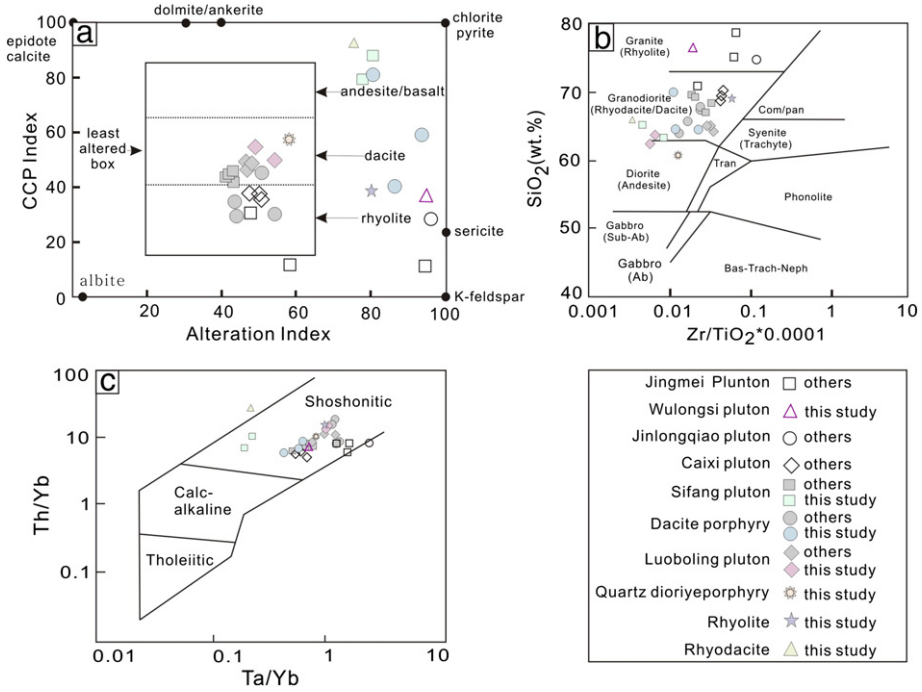

Fig. 10. a) Plots of the studied rocks on the alteration box diagram (Large et al., 2001). Inset box shows field of least altered rocks. Alteration Index = 100 * (K_2O + MgO) / (K_2O + MgO + Na_2O + CaO), chlorite-carbonate-pyrite (CCP) index = 100 * (MgO + FeO*) / (MgO + FeO* + Na_2O + K_2O). b) SiO_2 vs. Zr/TiO_2*0.0001 diagram for the Southeast ore segment (after Winchester and Floyd, 1977), data shown in grey and black collected from Zhao et al. (2007), Jiang et al. (2013)and Li et al. (2013b). c) Th/Yb vs. Ta/Yb diagram for the rocks in the Southeast ore segment (after Müller et al., 1992).

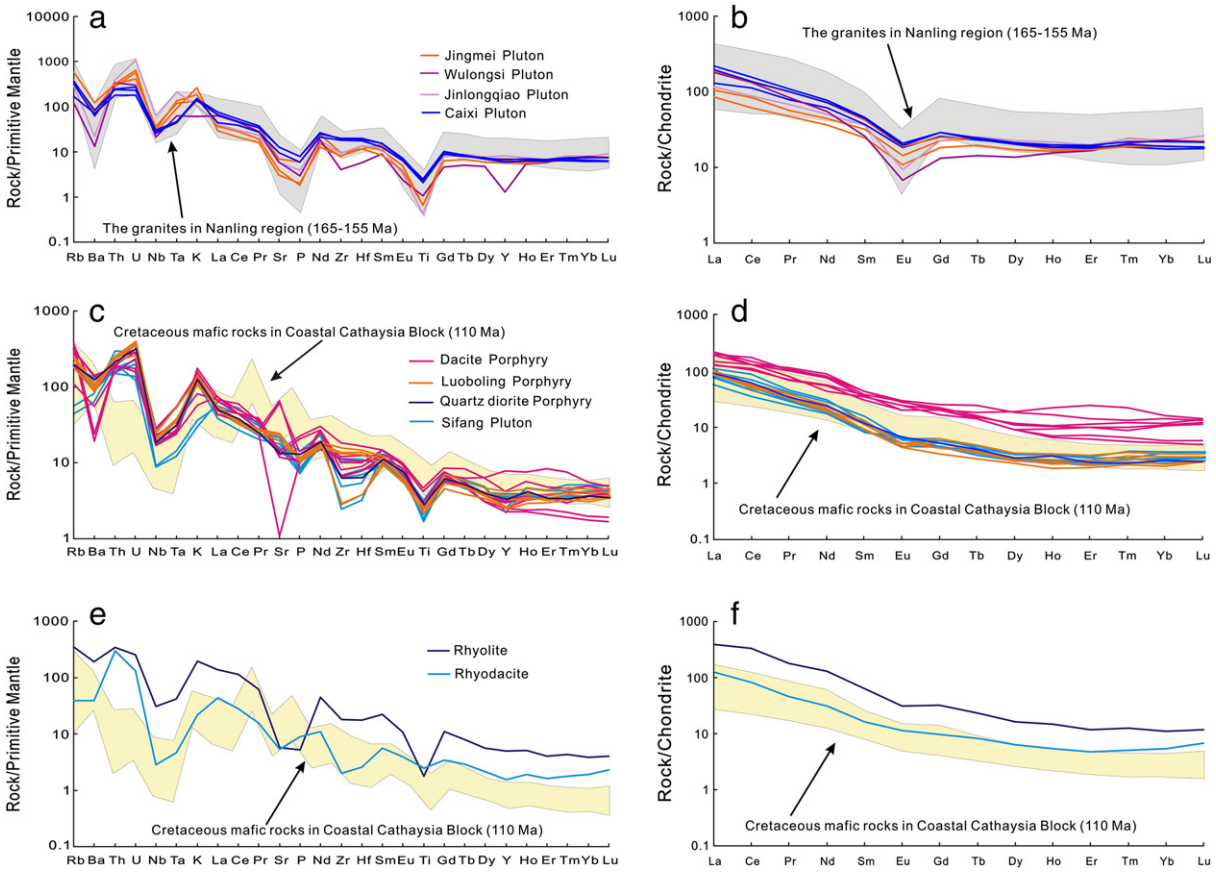

Fig. 11. Chondrite-normalized REE patterns and primitive mantle-normalized multi-element diagrams for the rocks from the SOE. The grey field is from the granites in Nanling region (Li et al., 2013a and the reference therein), and the yellow area represents mafic rocks from the Coastal Cathaysia Block (Chen et al., 2008). Data of average chondrite and primitive mantle are from Sun and McDonough (1989).

Based on the above discussion, we can conclude that the Middle to Late Jurassic magmatic event in the Zijinshan district ranges from 165 Ma to 150 Ma, during which time the Zijinshan granite complex and the Caixi pluton were emplaced. New data shows that the Cretaceous magmatic event in the Zijinshan district lasted for ~14 Ma between 110 Ma and 95 Ma, which differs from the range of 125 to 94 Ma suggested by Zhang et al. (2001), and 112 to 101 Ma by Jiang et al. (2013). The Cretaceous event can be further divided into the late Early Cretaceous event (110–105 Ma), which includes the Sifang granite, Luoboling granite porphyry, dacite porphyry and quartz diorite porphyry; and the early Late Cretaceous event (100–95 Ma), including the rhyodacite and rhyolite. The molybdenite Re—Os ages are consistent with the ages of the late Early Cretaceous rocks. Thus the Middle to Late Jurassic rocks, the late Early Cretaceous rocks and the early Late Cretaceous rocks can also be defined as the pre-, syn- and post-mineralization rocks, respectively.

6.2. Oxidation state of magmatic sequence

The zircon Ce^{IV}/Ce^{III} ratios are primarily used as measures of the oxidation of the state of the magma. The syn-mineralization magmas (including the Sifang pluton, Luoboling pluton, dacite porphyry and quartz diorite porphyry) have relatively high Ce^{IV}/Ce^{III} ratios compared to the pre-mineralization magmas (the Zijinshan granite complex) (Zhong, 2014) and post-mineralization (including rhyodacite and rhyolite), suggesting that the syn-mineralization magmatic activity is characterized by relatively higher fO_2 than the pre- and post-mineralization magmas (Fig. 12a). On the other hand, the Eu_N/Eu_N^* vs. Ce^{IV}/Ce^{III} and Eu_N/Eu_N^* vs. Ce_N/Ce_N^* zircon data of the syn-mineralization (P1 porphyry, P2 porphyry, D1 porphyry, D2 porphyry, Sifang pluton, and the quartz diorite porphyry) rocks from the SOE mainly plot within the range defined by zircon grains from ore related intrusions in northern Chile (Ballard et al., 2002; Muñoz et al., 2012) (Fig. 12b and c) whereas the post-mineralization rocks mainly plot outside the field of the circle region (Fig. 12b), showing that the syn-mineralization rocks have higher Eu_N/Eu_N^* and Ce^{IV}/Ce^{III} ratios than other rocks which cannot be effectively distinguished using the Ce_N/Ce_N^* ratios (Fig. 12c). Thus, we conclude that the pre- and post-mineralization rocks were derived from relatively reduced magmas, whereas syn-mineralization intrusions were derived from highly oxidized magmas, and the high fO_2 is probably a reliable indicator for the mineralization of the Zijinshan field.

6.3. Petrogenesis of SOE and Zijinshan magmatism

6.3.1. Magma of pre-mineralization activity (165–150 Ma)

Pre-mineralization magmas (the Zijinshan granite complex and Caixi monzogranite) have similar major and trace element geochemical characteristics, such as enrichment of LILE and LREEs, depletion of HFSEs and significant negative Eu anomalies. Furthermore, the Zijinshan granite complex and Caixi monzogranite have similar characteristics to contemporaneous granites in the Nanling region (Fig. 11). The lower total REE contents (100–222 ppm) but enrichment of LREE, and higher Th and U contents (Th = 15–32 ppm, U = 4–22 ppm) indicate that the crustal materials may have played a significant role in the origin of Zijinshan pre-mineralization rocks (Tchameni et al., 2001; Upadhyay et al., 2006).

Table 5
Zircon trace elements of rocks from SOE.

	La	Ce	Pr	Nd	Sm	Eu	Gd	Tb	Dy	Ho	Er	Tm	Yb	Lu	Hf	Ce^{4+}/Ce^{3+}	Ce_N/Ce_N^*	Eu_N/Eu_N^*
DN178																		
1	0.009	110.301	0.192	3.080	7.285	2.440	37.342	12.839	152.245	57.570	259.178	53.839	485.242	100.831	9344.766	122	662	0.5
2	0.012	105.453	0.210	3.362	5.914	2.086	33.420	10.859	132.350	50.554	231.635	48.601	445.609	93.245	9506.513	164	525	0.5
3	0.152	75.461	0.440	7.104	11.654	3.440	54.507	16.746	183.769	65.667	279.381	56.291	504.091	102.777	9360.536	33	72	0.4
4	1.072	32.116	0.294	2.038	2.076	0.877	11.750	4.430	54.223	24.141	124.319	31.274	343.385	83.300	11,042.728	377	14	0.5
5	0.010	127.573	0.243	4.635	8.824	3.423	43.931	15.580	184.425	70.593	315.666	64.956	594.336	123.272	8672.905	118	623	0.5
6	0.016	96.866	0.182	3.499	5.808	2.030	32.359	10.313	119.340	45.658	202.574	41.951	379.900	78.825	9621.408	132	433	0.5
7	0.014	116.293	0.210	3.930	7.757	2.459	38.258	12.578	150.785	60.194	271.693	56.481	520.657	108.737	9042.985	124	529	0.4
8	0.043	65.768	0.561	9.165	14.495	4.515	62.865	18.856	203.549	71.480	299.379	59.291	523.238	104.991	9208.321	19	103	0.5
9	0.036	103.323	0.430	6.619	11.249	3.548	51.640	16.062	182.494	67.289	289.754	58.757	524.664	106.516	8896.527	51	204	0.4
10	0.020	117.330	0.307	4.586	9.102	2.920	46.087	13.961	152.711	54.265	220.894	43.659	380.718	75.781	8906.163	62	368	0.4
11	0.037	150.745	0.304	5.846	10.811	3.608	55.937	17.914	199.133	72.503	310.177	63.053	559.660	114.745	9398.650	86	347	0.4
12	14.351	119.267	4.280	19.671	7.665	2.031	29.596	9.554	111.111	42.294	190.635	40.875	369.384	76.728	10,352.259	94	4	0.4
13	0.024	106.629	0.211	3.811	7.188	2.493	37.438	12.562	143.700	56.445	248.198	52.524	475.932	98.586	9131.356	119	368	0.5
14	0.027	93.654	0.241	4.811	8.578	3.245	45.544	14.389	164.062	61.368	268.220	55.942	510.317	107.661	8202.892	80	283	0.5
15	0.116	62.985	0.857	13.339	20.422	6.713	81.995	23.583	239.707	82.392	332.112	64.984	557.415	112.563	8569.836	9	49	0.5
16	0.034	115.467	0.224	3.796	6.889	2.644	41.276	13.562	162.911	62.442	282.572	59.640	553.163	115.336	9475.524	163	323	0.5
17	0.047	83.845	0.317	5.154	11.059	3.263	47.520	13.997	153.711	54.899	234.766	47.704	427.032	87.404	8580.711	35	168	0.4
18	0.017	130.642	0.406	7.052	11.246	3.989	56.193	16.668	182.955	64.417	268.538	52.861	452.997	91.358	8162.771	55	388	0.5
19	0.031	84.081	0.349	5.698	8.174	3.572	38.873	12.032	142.858	53.876	232.667	47.901	430.169	89.601	7917.867	66	197	0.6
20	0.359	86.149	0.461	6.190	10.735	3.617	50.101	15.521	173.629	63.771	274.792	57.076	518.359	107.753	8905.798	47	52	0.5
21	0.025	127.480	0.306	4.781	9.669	2.975	47.492	15.952	178.846	68.303	298.953	61.735	556.236	113.457	9135.730	91	360	0.4
22	0.135	84.803	0.528	6.765	11.214	3.913	47.474	14.840	164.480	60.582	261.909	54.199	485.613	101.800	8266.647	40	78	0.5
DN090																		
1	0.005	138.444	0.253	3.767	8.613	2.466	44.667	14.305	166.219	62.634	278.623	58.733	530.461	109.056	9881.108	265	915	0.4
2	0.074	98.416	0.824	13.523	19.959	6.688	91.087	26.452	277.933	98.174	404.465	80.556	697.098	139.571	9001.426	45	98	0.5
3	0.033	88.870	0.234	4.334	8.222	2.744	40.129	13.292	158.876	61.351	274.178	56.008	512.315	105.852	8273.038	181	248	0.5
4	0.148	100.760	0.340	5.040	8.256	2.807	39.210	12.853	144.289	52.628	227.679	45.858	402.578	82.789	8771.549	159	110	0.5
5	0.021	53.961	0.347	5.883	9.545	3.230	42.159	12.354	136.165	47.631	204.643	41.514	371.445	77.846	8828.511	60	153	0.5
6	3.919	148.655	1.216	8.961	9.443	2.816	45.082	14.950	176.669	68.590	312.601	66.373	623.818	128.271	9649.692	281	17	0.4
7	0.351	68.032	0.781	10.983	17.976	6.474	73.680	20.494	207.017	70.446	286.461	55.531	479.460	97.341	8719.600	26	32	0.5
8	4.754	114.510	1.522	10.143	9.630	3.167	42.979	13.037	146.395	54.770	240.743	49.497	438.563	90.552	9164.146	148	10	0.5
9	0.360	56.990	0.410	6.139	10.316	2.922	44.279	13.052	142.857	50.402	212.347	43.251	385.943	78.048	9206.910	55	36	0.4
10	0.065	74.832	0.618	9.755	15.552	5.287	64.483	18.950	201.313	71.087	295.331	60.124	518.725	105.598	8529.545	43	92	0.5
11	0.017	80.388	0.132	3.374	6.066	1.968	28.966	9.422	108.683	40.981	183.388	37.965	345.422	70.939	9570.023	203	416	0.5
12	0.019	128.739	0.261	4.905	9.207	3.074	43.973	13.657	159.621	56.807	246.298	49.375	438.335	88.890	9216.834	175	446	0.5
13	0.049	105.325	0.406	6.022	9.672	3.613	48.483	14.999	165.973	59.559	253.640	50.096	432.752	87.357	8259.804	127	184	0.5
14	0.023	114.324	0.196	2.927	6.468	1.955	35.532	11.448	136.458	51.211	233.387	48.453	453.299	92.642	10,266.216	328	419	0.4
15	0.032	100.510	0.169	2.313	5.072	1.651	30.769	10.514	126.345	50.700	240.591	52.407	504.283	107.464	10,606.787	545	333	0.4
DN040																		
1	10.995	40.134	2.638	11.119	3.274	0.976	10.897	3.979	54.580	24.322	129.507	32.804	361.977	90.710	11,505.999	530	2	0.5
2	0.017	35.477	0.028	0.767	2.564	1.192	15.607	5.999	84.241	36.961	195.671	48.894	519.150	125.444	11,061.333	987	396	0.6
3	0.264	21.135	0.111	0.726	1.103	0.803	10.697	3.797	56.266	25.759	140.310	35.362	400.461	100.796	11,590.574	2486	30	0.7
4	1.352	25.533	0.389	2.147	2.073	1.123	12.953	4.870	65.603	30.172	163.880	41.384	470.036	120.427	11,669.723	1061	9	0.7
5	4.920	35.724	1.412	7.162	3.744	1.250	14.870	5.572	70.919	31.823	168.363	42.317	475.308	117.782	11,567.058	463	3	0.5
6	0.094	27.571	0.063	1.059	2.212	0.976	10.365	4.074	53.574	23.609	123.044	30.240	325.592	79.147	11,255.118	668	88	0.6
7	0.007	25.435	0.056	0.649	2.019	0.956	14.868	5.461	73.912	31.646	169.065	41.392	462.482	112.270	11,470.528	1013	325	0.5
8	0.003	27.097	0.042	0.733	2.050	1.035	15.029	5.659	77.411	34.621	187.158	46.934	518.944	125.863	11,345.468	1175	569	0.6
9	0.504	38.356	0.180	1.407	2.412	1.201	15.389	6.214	84.492	37.899	203.686	52.064	561.520	135.376	11,143.325	1301	31	0.6
10	0.003	28.098	0.036	0.835	1.976	0.999	13.252	5.257	72.572	33.586	176.460	44.443	485.990	121.947	11,327.043	1277	619	0.6
11	0.007	20.777	0.010	0.493	1.433	0.724	9.983	3.854	52.950	24.358	135.366	34.145	385.250	97.822	11,724.726	1450	621	0.6
12	8.825	49.513	2.538	13.953	7.699	2.782	31.686	9.316	104.116	38.837	175.632	39.357	393.945	93.467	11,341.490	118	3	0.5
13	0.037	27.865	0.043	0.716	1.607	0.826	11.294	4.264	61.129	27.792	153.412	39.497	444.209	114.120	11,679.336	1800	170	0.6

(continued on next page)

Table 5 (*continued*)

	La	Ce	Pr	Nd	Sm	Eu	Gd	Tb	Dy	Ho	Er	Tm	Yb	Lu	Hf	Ce^{4+}/Ce^{3+}	Ce_N/Ce_N^*	Eu_N/Eu_N^*
14	0.021	34.937	0.059	0.643	2.302	1.009	15.431	5.486	76.226	32.757	174.007	42.825	458.137	111.915	11,097.729	1074	240	0.5
15	0.043	16.515	0.030	0.763	1.583	0.819	11.559	4.147	57.392	24.741	132.750	32.597	354.262	87.969	11,636.995	840	113	0.6
16	0.007	15.841	0.017	0.276	1.028	0.599	8.327	3.084	42.405	19.342	105.406	26.771	297.878	74.902	11,747.870	1622	364	0.6
17	0.082	26.544	0.070	1.636	3.088	1.255	17.625	6.112	78.601	33.149	169.625	41.789	447.256	108.128	10,833.817	446	86	0.5
DN117																		
1	0.014	28.797	0.042	0.590	1.881	0.910	12.222	4.772	62.543	28.105	153.187	38.793	421.521	107.775	11,191.412	668	289	0.6
2	0.333	36.965	0.126	0.966	2.364	1.183	16.356	6.303	87.723	39.946	212.417	53.606	579.600	144.460	11,060.410	718	44	0.6
3	0.016	23.533	0.082	1.309	3.053	1.255	15.415	5.795	71.819	31.557	167.895	42.495	467.828	119.238	11,367.984	235	158	0.6
4	0.004	32.205	0.013	0.846	1.955	0.859	12.365	5.053	72.153	33.234	186.203	47.712	531.601	136.087	11,261.665	870	1148	0.5
5	0.003	50.099	0.045	0.923	2.666	1.310	17.535	6.861	93.293	42.608	229.007	57.774	629.012	158.861	11,393.531	848	1007	0.6
6	0.003	30.750	0.023	0.927	1.682	0.875	11.649	4.774	67.573	31.880	177.987	46.715	521.714	134.267	11,237.277	1103	870	0.6
7	0.021	22.471	0.026	0.511	1.205	0.662	9.366	3.457	51.078	23.232	130.819	33.513	380.737	98.096	11,546.465	1140	239	0.6
8	0.007	25.775	0.022	0.771	1.248	0.823	11.125	4.142	54.585	25.810	145.355	38.079	427.806	110.577	11,380.646	1374	517	0.7
9	0.007	38.322	0.035	0.618	1.994	1.073	13.637	4.876	68.733	29.359	161.111	40.577	443.838	110.242	11,380.122	803	617	0.6
10	0.000	26.062	0.030	0.578	1.405	0.722	9.566	3.563	48.845	21.497	116.131	29.562	335.597	84.269	11,420.605	622	411	0.6
11	0.013	40.342	0.067	1.155	2.218	1.193	16.713	6.739	92.196	42.127	224.423	56.138	626.558	157.853	11,303.023	966	334	0.6
12	0.051	28.980	0.041	0.626	1.364	0.739	11.216	4.204	58.823	27.155	146.867	37.807	419.340	106.291	11,305.630	1236	156	0.6
DN138																		
1	0.204	37.389	1.709	1.486	2.486	0.641	8.722	2.886	40.006	17.550	93.938	24.293	273.991	69.178	11,583.551	427	16	0.4
2	0.051	27.835	0.066	0.792	1.876	0.770	10.468	4.021	51.891	24.068	123.636	32.085	352.532	87.653	11,252.752	672	118	0.5
3	0.010	26.837	0.061	0.945	1.875	0.813	10.725	3.951	49.629	22.019	116.419	28.747	316.623	78.257	10,787.174	579	264	0.6
4	1.404	25.385	0.327	1.836	1.664	0.761	9.439	3.506	44.073	19.278	100.167	25.042	272.806	67.127	11,253.990	595	9	0.6
5	0.003	23.556	0.044	0.556	1.630	0.592	8.872	3.282	42.758	18.628	101.449	26.261	289.059	72.057	11,171.491	622	471	0.5
6	0.003	24.677	0.020	0.844	1.500	0.661	9.168	3.459	49.807	21.568	116.479	29.863	330.772	81.856	11,349.011	855	758	0.5
7	0.007	17.558	0.028	0.609	1.190	0.665	7.831	3.017	39.027	16.940	92.712	23.311	262.445	65.418	11,240.317	774	316	0.7
8	49.200	116.997	10.286	41.491	7.590	1.516	13.457	3.877	46.162	19.602	98.919	24.425	264.482	64.667	11,149.709	143	1	0.5
9	0.024	31.132	0.021	0.914	2.403	0.923	11.851	4.354	58.805	25.953	137.071	34.817	388.186	94.467	10,924.641	498	343	0.5
10	3.283	28.810	0.697	5.649	2.321	0.619	10.455	3.418	45.786	19.817	104.700	26.370	288.142	70.199	11,241.362	372	5	0.4
11	95.031	197.330	18.662	72.778	11.471	2.134	15.309	3.923	49.189	20.015	100.437	25.392	272.499	67.759	10,885.409	114	1	0.5
DN291																		
1	0.004	28.435	0.075	0.730	1.759	0.835	10.190	3.642	48.511	21.265	113.635	28.355	307.951	77.872	10,527.040	815	430	0.6
2	0.034	26.145	0.054	0.685	1.837	0.778	9.676	3.607	49.434	22.026	116.197	29.785	322.039	81.208	11,167.497	719	150	0.6
3	16.000	55.976	3.388	13.509	3.542	0.968	11.312	3.716	48.618	19.846	102.321	26.006	272.417	67.455	11,545.467	361	2	0.5
4	0.004	23.388	0.032	0.495	1.351	0.621	9.761	3.377	45.122	19.711	104.216	26.407	290.364	72.385	11,461.900	1039	522	0.5
5	8.042	37.344	1.633	6.873	2.191	0.705	9.500	3.276	44.591	19.291	105.269	26.743	300.602	75.040	11,702.330	685	3	0.5
6	0.620	30.522	0.155	1.702	2.133	0.928	11.855	4.121	56.409	24.091	128.589	33.015	361.208	89.760	10,987.911	688	24	0.6
7	1.326	22.386	0.237	1.509	1.592	0.715	9.081	3.299	47.508	20.129	108.190	26.955	297.607	72.720	11,359.335	724	10	0.6
8	0.561	27.775	0.129	1.224	1.825	0.632	10.224	3.485	49.203	21.292	115.144	29.406	320.150	79.840	11,115.713	760	25	0.4
9	0.028	28.877	0.054	0.907	1.793	0.783	11.657	4.413	60.168	26.012	137.077	34.278	376.026	91.845	11,292.990	920	181	0.5
10	0.003	23.087	0.026	0.571	1.658	0.655	8.646	3.082	39.140	16.984	86.547	22.267	239.043	57.483	11,670.125	554	659	0.5
11	0.064	30.973	0.083	0.859	2.146	0.950	11.473	3.847	49.947	21.746	114.684	27.983	298.626	72.044	11,008.619	556	104	0.6
12	4.241	29.802	1.044	4.783	1.886	0.808	9.081	3.171	41.886	18.577	97.762	24.918	271.234	68.002	11,779.286	662	3	0.6
13	0.007	25.376	0.060	0.821	1.937	0.931	12.015	4.227	52.783	23.611	125.237	31.758	348.661	85.380	11,192.748	658	297	0.6
14	0.150	28.356	0.070	0.669	2.189	0.863	12.233	4.503	58.932	24.851	127.341	30.352	335.738	79.135	11,592.396	528	68	0.5
15	0.032	28.999	0.043	0.684	1.911	0.894	9.663	4.028	52.959	22.578	118.619	29.968	325.538	78.487	11,456.025	706	192	0.6
16	15.300	50.891	3.430	12.640	3.344	0.926	8.478	2.752	35.077	14.900	76.273	18.563	204.878	49.627	11,499.587	277	2	0.5
DN196																		
1	0.786	26.808	0.282	1.534	1.977	0.975	12.283	4.708	63.149	28.589	154.508	39.320	442.855	113.554	11,975.375	628	145	0.6
2	0.040	27.860	0.055	0.812	1.557	0.795	9.854	3.711	49.239	20.265	106.225	27.250	286.789	69.328	11,418.702	623	14	0.6
3	0.051	25.210	0.034	0.630	1.591	0.747	8.409	3.339	46.328	20.631	111.229	27.754	312.186	77.225	11,225.331	617	150	0.6
4	0.003	23.771	0.029	0.501	1.873	0.840	10.404	4.027	51.186	22.630	118.528	30.292	338.907	84.060	12,351.380	459	620	0.6
5	0.088	28.809	0.049	0.754	1.685	0.836	9.915	3.661	47.802	20.617	105.929	26.257	290.067	70.534	11,314.261	571	107	0.6
6	0.020	29.119	0.060	0.992	2.005	0.991	12.329	4.429	57.497	25.063	133.646	33.454	367.430	89.997	11,422.118	522	208	0.6
7	0.082	28.599	0.048	0.783	1.800	0.776	10.291	3.822	48.061	20.922	109.551	26.949	289.992	70.575	11,319.875	499	111	0.6

8	0.003	30.274	0.042	0.828	2.197	1.083	14.080	5.030	65.994	28.506	152.739	38.518	416.268	101.713	11,229.955	508	655	0.6
9	4.004	34.795	1.128	5.613	3.003	1.151	14.266	5.041	64.697	27.707	140.730	34.455	360.003	85.533	11,848.842	267	4	0.5
10	0.003	20.515	0.016	0.640	1.554	0.743	7.511	3.080	38.560	17.256	93.022	24.126	265.891	66.891	11,643.374	464	723	0.7
11	0.006	27.885	0.021	0.761	1.849	0.960	12.771	4.810	66.481	30.180	164.828	42.245	473.812	120.605	12,223.727	779	622	0.6
12	0.007	18.242	0.015	0.545	1.077	0.618	8.287	3.406	48.402	21.522	118.194	29.795	328.198	82.073	11,630.614	998	437	0.6
13	0.003	26.132	0.021	0.678	1.557	0.861	10.861	4.143	53.500	23.699	131.077	33.741	371.580	92.301	11,414.177	789	764	0.6
14	0.003	17.692	0.029	0.777	1.904	0.768	12.159	4.472	58.391	25.026	133.509	33.391	366.487	93.358	12,104.013	363	435	0.5
15	0.004	18.534	0.011	0.431	0.914	0.624	7.447	3.046	42.405	20.491	115.192	30.394	359.256	93.406	12,121.985	1627	740	0.7
16	0.044	17.072	0.057	0.501	1.548	0.751	8.810	3.343	44.118	20.035	109.763	27.730	317.054	82.609	12,016.012	476	84	0.6
17	0.006	29.863	0.058	0.828	2.127	0.956	13.135	4.869	66.488	29.512	160.268	40.142	448.191	112.110	11,521.264	591	388	0.6
DN054																		
1	0.054	13.442	0.030	0.467	0.906	0.424	5.407	1.995	26.542	11.842	62.484	15.930	173.435	43.026	4566.948	841	81	0.6
2	0.001	10.812	0.016	0.288	0.690	0.269	3.952	1.343	17.669	7.627	39.304	9.949	105.455	26.186	4681.844	715	592	0.5
3	0.045	11.703	0.027	0.367	0.738	0.290	4.378	1.575	20.972	9.053	46.737	11.482	124.174	30.394	4680.006	777	82	0.5
4	0.002	11.218	0.017	0.380	0.675	0.298	3.856	1.362	17.496	7.492	39.050	9.876	106.488	26.172	4673.622	773	538	0.6
5	0.003	11.064	0.029	0.526	1.191	0.504	5.747	2.062	26.114	11.471	59.266	14.593	157.490	38.838	4603.451	368	280	0.6
6	0.411	10.709	0.094	0.646	0.786	0.322	4.488	1.610	20.795	8.975	47.447	12.057	130.968	32.705	4702.101	682	13	0.5
7	0.002	10.790	0.019	0.343	0.711	0.263	3.998	1.366	17.637	7.750	39.803	10.040	107.376	26.819	4609.676	691	406	0.5
8	0.175	10.835	0.068	0.818	1.577	0.568	7.396	2.345	29.267	11.899	59.303	14.102	146.395	35.420	4716.340	188	24	0.5
9	0.002	12.587	0.022	0.347	1.048	0.420	5.582	2.063	26.986	11.869	60.922	15.241	161.642	39.879	4659.024	548	535	0.5
10	0.080	14.286	0.041	0.453	0.809	0.389	5.042	1.873	24.412	10.857	57.543	14.613	156.888	39.084	4624.531	1017	62	0.6
11	0.018	10.630	0.062	1.061	2.119	0.864	10.037	3.234	36.408	14.446	69.190	16.512	170.910	41.693	4888.795	120	78	0.6
12	2.389	16.476	0.473	2.114	0.990	0.355	4.058	1.392	17.715	7.539	38.450	9.453	100.138	24.582	4707.126	511	4	0.5
13	0.029	11.373	0.075	1.350	2.102	0.842	9.581	2.966	33.505	13.109	63.082	14.722	149.363	36.169	4576.164	113	59	0.6
14	0.006	10.265	0.032	0.677	1.298	0.530	6.090	2.202	26.721	11.202	56.397	13.648	144.526	35.122	4692.463	260	179	0.6
15	0.007	8.639	0.052	0.712	1.378	0.680	6.202	2.101	25.896	10.410	52.145	12.282	129.278	31.723	4421.298	175	110	0.7
16	2.816	15.701	0.626	2.593	1.013	0.323	4.002	1.374	17.385	7.481	38.156	9.597	101.619	24.872	4810.245	473	3	0.5
17	0.036	7.891	0.016	0.239	0.515	0.268	3.377	1.236	16.449	7.320	39.045	10.050	111.762	28.822	5140.806	1021	80	0.6

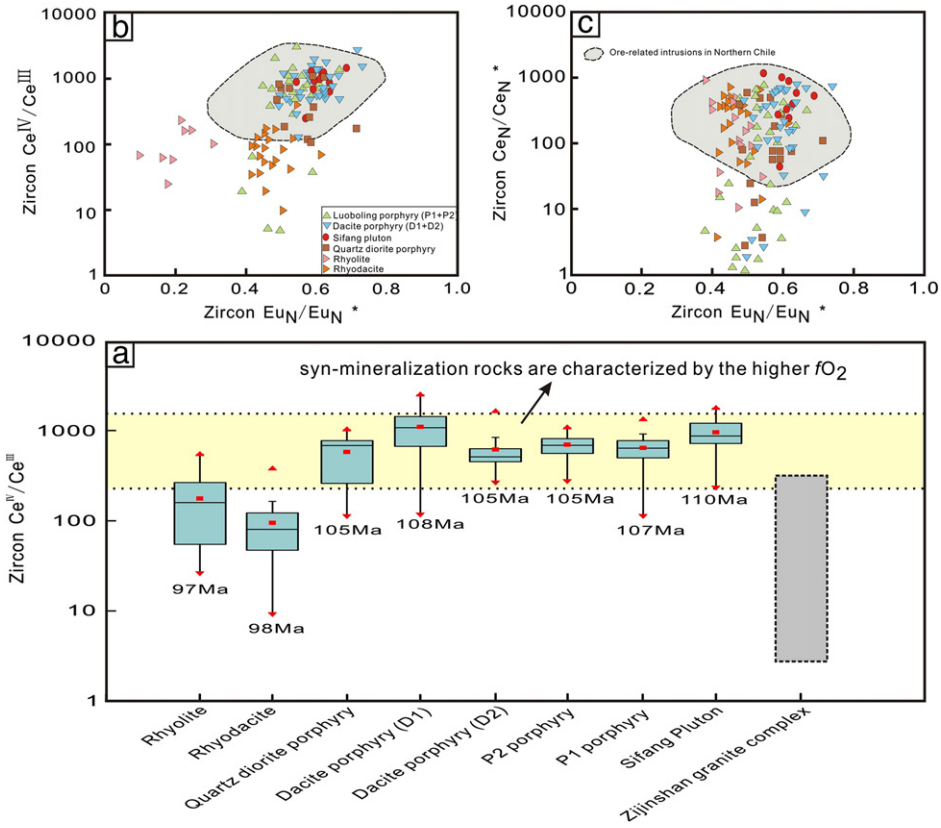

Fig. 12. a) Zircon Ce^{IV}/Ce^{III} ratios for rocks in the Southeast ore segment (data for the grey bar on the right for the Zijinshan granite complex are from Zhong, 2014). b) Zircon Ce^{IV}/Ce^{III} vs. Eu_N/Eu_N* c) Ce_N/Ce_N* vs. Eu_N/Eu_N*. Diagrams constructed using individual zircons from igneous rocks in SOE. The data range of ore-related intrusions in Northern Chile is from Ballard et al. (2002) and Muñoz et al. (2012).

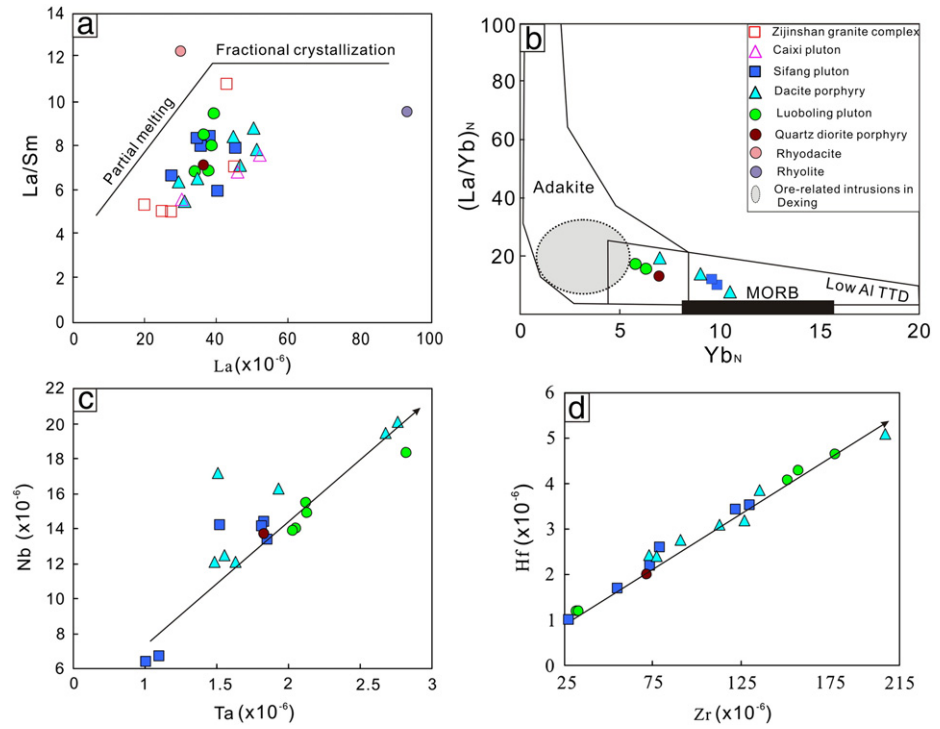

Fig. 13. a) La/Sm vs. La diagram. b) Plots of Yb_N vs. $(La/Yb)_N$ for the igneous rocks in the Zijinshan Orefield. The diagrams are modified after Defant and Drummond (1990, 1993). Ore-related porphyry data is from Dexing from Wang et al. (2006). c) Nb vs. Ta diagram. d) Hf vs. Zr diagram. Additional data for the Zijinshan complex is from Jiang et al. (2013).

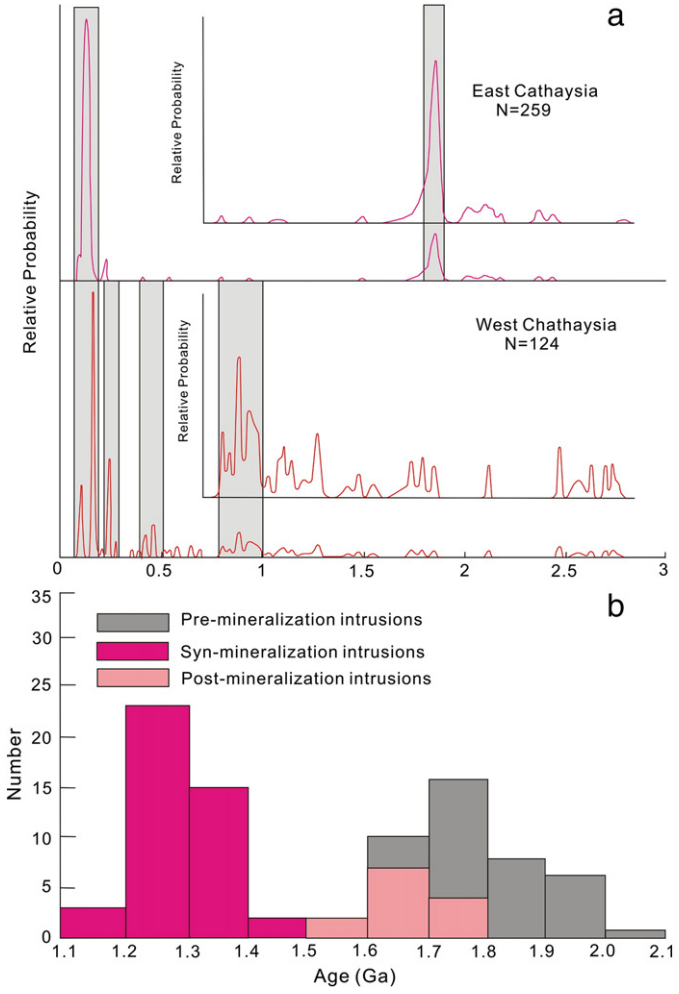

Fig. 14. Hf isotope crustal model age (T_{DM2}) histogram for zircon grains from the SOE. The data for the Western Cathaysia and Eastern Cathaysia blocks from Xu et al. (2007). The data range for the pre-mineralization intrusions is from Li et al. (2015).

The Zijinshan granite complex and the Caixi monzogranite show positive correlation between La and La/Sm (Fig. 13a), suggesting that compositional variation of the pre-mineralization magmatism is mainly controlled by partial melting (Barberi et al., 1975). Experimental studies have shown that partial melting of basaltic lower crust will generate melts with Mg# values of <40, irrespective of the degree of partial melting (Rapp et al., 1991; Rapp and Watson, 1995). The Mg# for the magma of pre-mineralization activities are lower than 40 (i.e. Mg# = 22 − 36), suggesting they were derived from the melting of mafic lower crust.

The crust of the Cathaysia block can be divided into the eastern Cathaysia and the western Cathaysia (Chen and Jahn, 1998). The boundary between the two is roughly along the Zhenghe-Dapu fault as defined by Chen and Jahn (1998), placing the Zijinshan district in western Cathaysia. The basement of eastern Cathaysia is dominantly Paleoproterozoic (1850–1870 Ma, 2100–2400 Ma) in age with minor Archean components, whereas the crust of western Cathaysia was generated mainly during the Neoproterozoic, although it contains some Archean (2500–3500 Ma) to Mesoproterozoic components (Fig. 14a; Xu et al., 2007). According to Xu et al. (2007), the Neoproterozoic crust itself represents a mixture of sources that involved both juvenile components and the reworked Paleo- to Mesoproterozoic crust. The Hf model ages of Neoproterozoic zircons mainly range from 2.1 Ga to 1.4 Ga (Xu et al., 2007), similar to the T_{DM2} ages (2.1–1.6 Ga; Li et al., 2015) for the Middle to Late Jurassic rocks at Zijinshan (Fig. 14b). Furthermore, the $\varepsilon_{Hf}(t)$ for the pre-mineralization rocks lie below the 1.4 Ga crustal evolution line (Fig. 15), consistent with a crustal source for the pre-mineralization activity. Thus, it is likely that the mixing of juvenile components and the reworking of Paleo- to Mesoproterozoic crust produced the Neoproterozoic crust of western Cathaysia, which in turn served as the source for the Middle to Late Jurassic magma in the Zijinshan district.

6.3.2. Magma of syn-mineralization activity and post-mineralization activity (110–95 Ma)

The syn- (110–105 Ma; including the Sifang pluton, the Luoboling pluton, dacite porphyry and quartz diorite porphyry) and post-mineralization magmas (100–95 Ma; including rhyolite and rhyodacite) are characterized by high SiO_2 (average = 67 wt.%) and relatively high Mg# (average = 40). As shown in Fig. 13a, the late Early Cretaceous intrusions may have been formed by significant degrees of partial melting. Thus the high Mg# may suggest a greater role mantle materials compared to the Middle to Late Jurassic intrusions. The ca. 1849 Ma zircon from the P3 porphyry also suggests that the Cathaysia Block basement may have played a role in the source of the Cretaceous magma.

The zircons from the syn- and post-mineralization rocks show Hf model ages (Fig. 14b) ranging from 1.8 Ga to 1.0 Ga, younger than the model ages of the Middle to Late Jurassic rocks in the Zijinshan district, suggesting a higher proportion of juvenile mantle. The $\varepsilon_{Hf}(t)$ are above the 1.4 Ga crustal evolution line (Fig. 15), further precluding the crust as the only source for the syn-mineralization activity. Furthermore, the high total REE content (124–399 ppm), the existence of the mafic microgranular enclaves in the syn-mineralization intrusions (Fig. 15), and the heterogeneous Hf isotopic compositions ($\varepsilon_{Hf}(t)$ range of −9.4 to −0.9) of zircons from the rhyodacite (Fig. 15) also suggest magma

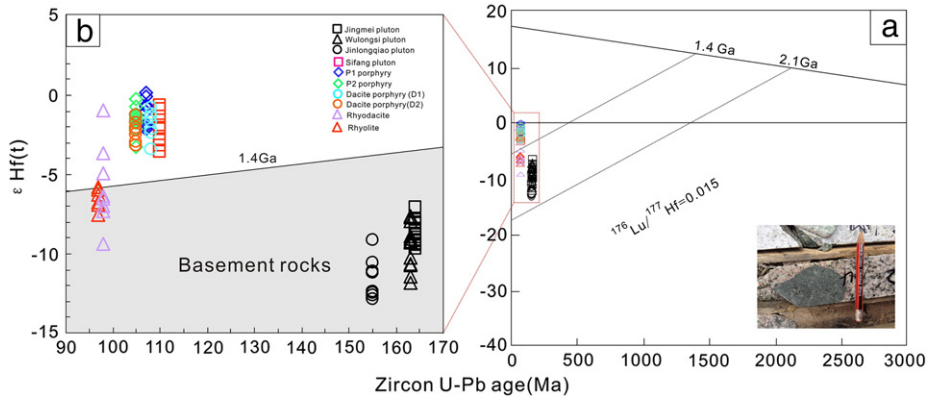

Fig. 15. Zircon Hf isotopic compositions of the SOE. The photograph shows the existence of the mafic microgranular enclaves in the Luoboling granodiorite. The data ranges for the Jingmei pluton, Wulongsi pluton and Jinlongqiao pluton are from Li et al. (2015).

mixing. Therefore, it is likely that a significant amount of mantle material was involved in the generation of syn-mineralization and post-mineralization activity compared to the pre-mineralization magmatism. The zircon Hf isotopic compositions of the post-mineralization magmas are enriched relative to the syn-mineralization intrusions (Fig. 15). The ε_{Hf} (t) values for the syn-mineralization activity are between −3.6 to 0.1, whereas post-mineralization trachy-andesite and rhyolite have ε_{Hf} (t) values ranging from −7.5 to −5.8, −9.4 to −0.9, respectively, suggesting that post-mineralization activity involved more crustal material in the source than the syn-mineralization activity (Fig. 15).

As discussed before, the syn-mineralization magma is characterized by the higher oxygen fugacities than the pre- and post-mineralization magma. Subducted oceanic crust has variable but locally very high intrinsic fO_2 due to equilibration with seawater during hydrothermal alteration and deposition of terrigenous sediment (Mungall, 2002). Melts or fluids derived from the slab will carry this oxidizing potential up into the overlying mantle (e.g., McInnes and Cameron, 1994). So the high oxygen fugacity of the syn-mineralization rocks may be related to subducted oceanic crust. Furthermore, the syn-mineralization rocks are characterized by strong enrichment of LILEs and depletion of the HFSEs, with negative Ta—Nb and Ti anomalies (Fig. 11), which are common features of the contemporaneous Cretaceous mafic suites in the Cathaysia Block that are interpreted to have been generated by partial melting of subcontinental lithosphere metasomatised by slab-induced fluids and/or melts (Chen et al., 2008; Meng et al., 2012). Thus the slab-induced fluids and/or melts may have played an important role in the formation of the syn-mineralization magma.

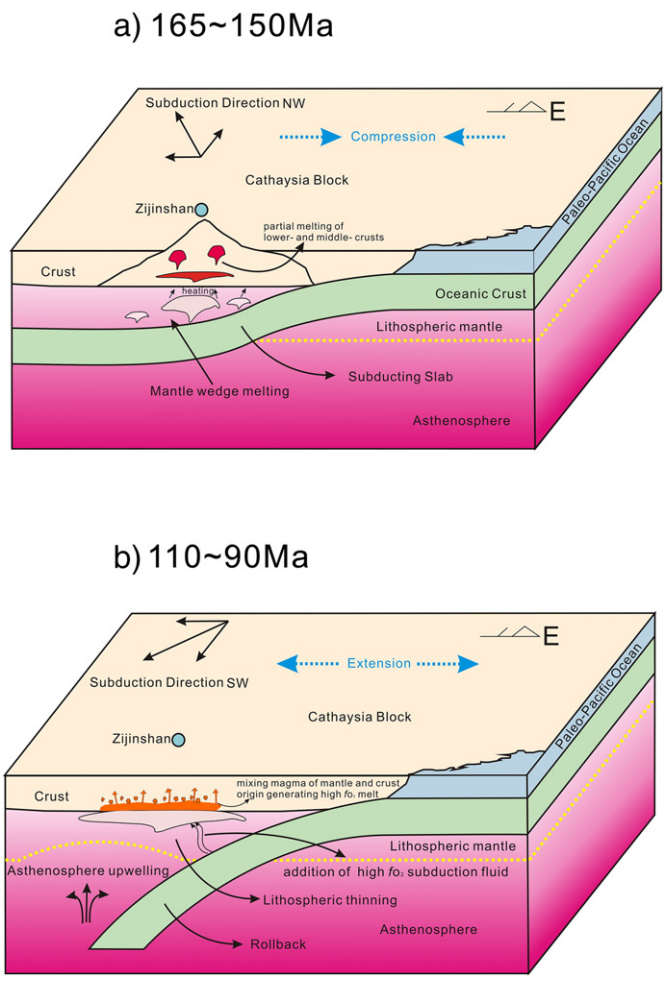

Fig. 16. Schematic geodynamic model of the Southeast Ore Segment during the Jurassic and Cretaceous (Modified after Sun et al., 2008).

During the subduction process, the slab component will be transferred into aqueous fluids, hydrous melts or supercritical liquids (Kessel et al., 2005). In order to further investigate whether the high fO_2 of the syn-mineralization magma was inherited from the slab-induced fluids or melts, we compared the syn-mineralization rocks in the Zijinshan district with the high fO_2 adakitic rocks in the Dexing porphyry Cu deposit (Wang et al., 2006).

The $(La/Yb)_N$ vs. Yb_N plot (Fig. 13b) show that the Luoboling pluton and the quartz diorite porphyry plot along the boundary between the adakite and the low Al TTD, but outside the field of the Dexing adakites, whereas the Sifang pluton and the dacite porphyry plot in the Low Al TTD field. Since the Luoboling pluton and Sifang pluton show atypical adakite affinity compared to those in Dexing, they were less likely to have formed from the partial melting of the subducted oceanic slab that has been proposed for the formation of the Dexing adakite (Wang et al., 2006; Zhou, 2011). Considering the high fO_2 and the lack of adakitic properties for the syn-mineralization rocks at Zijinshan, we suggest that the highly oxidized supercritical fluids from the subducted oceanic slab may have played an important role in generating the high fO_2 primary magma with weak adakite affinity, similar to the model proposed by Bissig et al. (2003) in the Central Andes and Wu et al. (2015) in the Halasu Cu belt, NW China. Furthermore, on the Zr vs. Hf and Nb vs. Ta plots (Fig. 13c and d), all syn-mineralization intrusions lie along the same trend, suggesting that they were likely derived from the same magmatic source.

The geochemical data from this study suggests that the pre-mineralization magmas were derived from the partial melting of the Cathaysia basement crust with low fO_2 whereas the syn-mineralization and post-mineralization magmas were generated by mixing of subduction-related high fO_2 metasomatized mantle and crustal melts, with less mantle component in the post-mineralization magma.

6.4. Geodynamic setting

The geodynamic setting of the Zijinshan mineral field has been the subject of considerable debate with a number of models proposed. Zhang et al. (2001) proposed that the Zijinshan district was in a compressional environment during the Middle to Late Jurassic but switched to an extensional setting during the Cretaceous, but the reason for the switch was not clear. Jiang et al. (2013) proposed that the Zijinshan district formed during Paleo-pacific subduction during the Middle to Late Jurassic and the Cretaceous, but did not address the question of whether it was under compression or extension.

In Southeast China, there are large scale nappe structures and a stratigraphic hiatus between the Middle Jurassic (J2) and overlying Early Cretaceous (K1), which suggests a general compressional environment during the Middle to Late Jurassic (Li and Li, 2015). The geochemical features of the Middle to Late Jurassic rocks at Zijinshan indicate that they formed in a supra-subduction environment. A recent zircon U—Pb age of 187 ± 1 Ma from the Early Jurassic Jincheng Granite in the Fujian Province has been used to suggest that the Paleo-Pacific plate started to subduct underneath Eurasia in the Jurassic (Zhou and Li, 2000; Li and Li, 2007; Liu et al., 2011). During subduction, melting of the mantle wedge and basaltic underplating of the crust provided the necessary heat to cause partial melting of the Cathaysia Block, and generation of voluminous felsic magmas at Zijinshan, including the Zijinshan granite complex and the Caixi pluton, which is consistent with the model proposed by Zhou and Li (2000) for the Mesozoic magma in Southeastern China. Circa 125 Ma ocean island chains suggest a northwest plate motion for the Paleo-Pacific plate (Sun et al., 2007), suggesting that in the Middle to Late Jurassic Southeast China was probably in a relatively compressional setting affected by the northwest subduction (Fig. 16a).

The presence of mantle-derived melts in the Cretaceous magmatic sequences (syn-mineralization rocks and post-mineralization rocks) suggests a switch to an extensional setting (Li, 2000). The large scale bimodal volcanism, basic dike swarms, and alkali granites during 110 Ma

to 80 Ma all support an extensional setting in South China during the Cretaceous (Li and Li, 2015). Upwelling of subduction-related asthenosphere is an effective way to generate extension and associated Early Cretaceous magmatism in the SE China continent (Jahn, 1974; Zhou and Li, 2000; Chen et al., 2008). Zhou and Li (2000) suggested that the magmatic activity along the Southeast China continental margin migrated southeast to the ocean as the slab dip angle of the Paleo-Pacific plate increased from very low to medium. Sun et al. (2007) and Li and Li (2015) proposed that changes in the direction of movement of the Paleo-Pacific plate may have generated two compressional and three extensional events in Southeast China during the Late Mesozoic. During the Middle to Late Jurassic, the subduction direction of the Paleo-pacific plate was northwest, and the direction changed multiple times. From ~110 Ma to ~100 Ma, the subduction direction of the Paleo-pacific plate was southwest (Sun et al., 2007; Li and Li, 2015)

Although the mechanism is still unknown, the changing of drift direction in the Early to Late Cretaceous may have cause slab rollback, inducing extension, lithosphere thinning and related magmatism (Fig. 16b), similar to that modelled for the Cenozoic Andes (Sobolev and Babeyko, 2005) and the Cretaceous North China craton (Sun et al., 2008).

The geochemistry of early Late Cretaceous (syn-mineralization) volcanic rocks suggests a greater crustal component than late Early Cretaceous (post-mineralization) rocks in the SOE at Zijinshan. Li (2000) proposed that magmatic activities dramatically declined at ~100 Ma in southeast China, which may suggest attenuated rollback of the subducted plate with weakening mantle source addition in the Late Cretaceous. That is consistent with a higher proportion of crustal materials in the source of the early Late Cretaceous rocks.

The following tectonic model is proposed for the Zijinshan district from 165–95 Ma (Fig. 16): (1) In the Middle to Late Jurassic (ca. 165–150 Ma), the Zijinshan district was under compression as a result of northwest subduction of the Pacific plate. During this time underplating by melts derived from the mantle wedge resulted in partial melting of the Cathaysia Block basement to form the Zijinshan granite complex and the Caixi pluton (Fig. 16a). (2) In the Cretaceous (110–95 Ma) a change in the direction of subduction from northwest to southwest put the Zijinshan district into extension. The change of subduction direction may have caused slab roll back and the subsequent upwelling of the asthenosphere (Fig. 16b). In the late Early Cretaceous (110–105 Ma), the upwelling asthenospheric mantle triggered the partial melting of the lithospheric mantle. With the addition of the highly oxidized supercritical fluids derived from the subducted slab, the primary magma was water-rich and highly oxidized. During ascent, the magma underwent crustal contamination to form the Sifang pluton, Luoboling pluton, dacite porphyry, and quartz diorite porphyry, together with the associated Cu—Mo mineralization. In the early Late Cretaceous (from 100 Ma to 95 Ma), the termination of slab rollback and a return to a more compressional environment would have reduced the mantle component and formed the rhyodacite and rhyolite.

7. Conclusions

1. LA-ICP-MS zircon U—Pb dating has identified two magmatic events in the Zijinshan district, a 165–150 Ma Middle to Late Jurassic and a Cretaceous event which can be divided into late Early Cretaceous rocks (110–105 Ma) and early Late Cretaceous rocks (100–95 Ma).
2. The late Early Cretaceous rocks formed from the mixing of subduction related metasomatized mantle derived high fO_2 melts with crustal melts, whereas the early Late Cretaceous rocks formed from a similar source but with a greater input of crustal materials. The Middle to Late Jurassic rocks were derived from the partial melting of crustal materials.
3. Molybdenite Re—Os ages and field relationships suggest that the late Early Cretaceous rocks (110 to 100 Ma) are coeval with mineralization in the SOE. So the Middle to Late Jurassic event, late Early Cretaceous event and the early Late Cretaceous event can also be defined as the pre-mineralization magmatic event, syn-mineralization magmatic event and the post-mineralization magmatic event.
4. The three magmatic events formed above the Paleo-Pacific Plate subduction zone beneath the Eurasian continent. The pre-mineralization activity formed in a compressional setting (165–150 Ma), and the syn-mineralization activity formed in a relatively extensional setting (110–105 Ma), but the post-mineralization activity once again became compressional (100–95 Ma) compared to the syn-mineralization activity.

Acknowledgements

We sincerely appreciate the detailed and constructive reviews and suggestions of Franco Pirajno and two anonymous reviewers, which greatly improved this paper. We thank the Zijin Mining Co. Ltd. for assisting the Field work. Congying Li and Shengling Sun is thanked for assisting the laboratory work. We sincerely appreciate the valuable suggestions offered by Huaying Liang and Wenting Huang. We sincerely appreciate the detailed suggestions of Jun. Zhong and Yanjing Chen. This research was financially supported by the Creative and interdisciplinary program, CAS (Y433131A07). This is contribution No.IS-2282 from GIGCAS.

References

Ballard, J.R., Palin, M.J., Campbell, I.H., 2002. Relative oxidation states of magmas inferred from Ce(IV)/Ce(III) in zircon: application to porphyry copper deposits of northern Chile. Contrib. Mineral. Petrol. 144, 347–364.
Barberi, F., Ferrara, G., Santacroce, R., Treuil, M., Varet, J., 1975. A transitional basalt-pantellerite sequence of fractional crystallization, the Boina Centre (Afar Rift, Ethiopia). J. Geol. 16, 22–56.
Belousova, E., Griffin, W.L., O'reilly, S.Y., Fisher, N.L., 2002. Igneous zircon: trace element composition as an indicator of source rock type. Contrib. Mineral. Petrol. 143, 602–622.
Bissig, T., Clark, A.H., Lee, J.K.W., Quadt, A.V., 2003. Petrogenetic and metallogenetic responses to Miocene slab flattening: new constraints from the El Indio-Pascua Au-Ag-Cu belt, Chile/Argentina. Mineral. Deposita 38, 844–862.
Bouvier, A., Vervoort, J.D., Patchett, P.J., 2008. The Lu-Hf and Sm-Nd isotopic composition of CHUR: constraints from unequilibrated chondrites and implications for the bulk composition of terrestrial planets. Earth Planet. Sci. Lett. 273, 48–57.
Chen, J.F., Jahn, B.M., 1998. Crustal evolution of southeastern China: Nd and Sr isotopic evidence. Tectonophysics 284, 101–133.
Chen, C.H., Lee, C.Y., Shinjo, R.I., 2008. Was there Jurassic paleo-Pacific subduction in South China?: constraints from ^{40}Ar-^{39}Ar dating, elemental and Sr-Nd-Pb isotopic geochemistry of the Mesozoic basalts. Lithos 106, 83–92.
Chen, J., Chen, Y.J., Zhong, J., Sun, Y., Li, J., Qi, J.P., Lu, Y.H., 2011. Fluid inclusion study of the Wuziqilong Cu deposit in the Zijinshan ore field, Fujian Province. Acta Petrol. Sin. 27, 1425–1438 (in Chinese with English abstract).
Chen, J., Chen, Y.J., Zhong, J., Sun, Y., Li, J., Qi, J.P., 2015. Geological and ore-fluid characteristics of Longjiangting Cu deposit in Zijinshan Orefield, Fujian Province, and their genetic implications. Mineral Deposits 34, 98–118 (in Chinese with English abstract).
Chu, N.C., Taylor, R.N., Chavagnae, V., Nesbitt, R.W., Boela, R.M., Milton, J.A., German, C.R., Bayon, G., Burton, K., 2002. Hf isotope ratio analysis using multi-collector inductively coupled plasma mass spectrometry: an evaluation of isobaric interference corrections. J. Anal. At. Spectrom. 17, 1567–1574.
Defant, M.J., Drummond, M.S., 1990. Derivation of some modern arc magmas by melting of young subducted lithosphere. Nature 347, 662–665.
Defant, M.J., Drummond, M.S., 1993. Mount St. Helens; potential example of the partial melting of the subducted lithosphere in a volcanic arc. Geology 21, 547–550.
Gao, T.J., 1999. Comparison of the Zijinshan copper-gold deposit and Circum-Pacific epithermal deposits. Geol. Fujian 18, 167–177 (in Chinese with English abstract).
Griffin, W.L., Wang, X., Jackson, S.E., Pearson, N.J., O'Reilly, S.Y., Xu, X.S., Zhou, X.M., 2002. Zircon chemistry and magma mixing, SE China: in-situ analysis of Hf isotopes, Tonglu and Pingtan igneous complexes. Lithos 61, 237–269.
Griffin, W.L., Belousova, E.A., Shee, S.R., Pearson, N.J., O'Reily, S.Y., 2004. Archean crustal evolution in the northern Yilgarn Craton: U-Pb and Hf-isotope evidence from detrital zircons. Precambrian Res. 13l, 23l–282.
Hua, R.M., Chen, P.R., Zhang, W.L., Yao, J.M., Lin, J.F., Zhang, Z.S., Gu, S.Y., 2005. Metallogeneses and their geodynamic settings related to mesozoic granitoids in the Nanling range. Geol. J. China Univ. 11, 291–304.
Huang, W.T., Li, J., Liang, H.Y., Wang, C.L., Lin, S.P., Wang, X.Z., 2013. Zircon LA-ICP-MS U-Pb ages and highly oxidized features of magma associated with Luoboling porphyry Cu-Mo deposit in Zijinshan ore field, Fujian Province. Acta Petrol. Sin. 29, 283–293 (in Chinese with English abstract).
Jahn, B.M., 1974. Mesozoic thermal events in southeast China. Nature 248, 480–483.
Jiang, S.H., Liang, Q.L., Bagas, L., Wang, S.H., Nie, F.J., Liu, Y.F., 2013. Geodynamic setting of the Zijinshan porphyry-epithermal Cu-Au-Mo-Ag ore system, SW Fujian Province,

China: constraints from the geochronology and geochemistry of the igneous rocks. Ore Geol. Rev. 53, 287–305.
Kessel, R., Schmidt, M.W., Ulmer, P., Pettke, P., 2005. Trace element signature of subduction-zone fluids, melts and supercritical liquids at 120–180 km depth. Nature 437, 724–727.
Large, R.R., Gemmell, J.B., Paulick, H., Huston, D.L., 2001. The alteration box plot: a simple approach to understanding the relationship between alteration mineralogy and lithogeochemistry associated with volcanichosted massive sulfide deposits. Econ. Geol. 96, 957–971.
Li, X.H., 2000. Cretaceous magmatism and lithospheric extension in Southeast China. J. Asian Earth Sci. 18, 293–305.
Li, B., Jiang, S.Y., 2014a. A subduction-related metasomatically enriched mantle origin for the Luoboling and Zhongliao Cretaceous granitoids from South China: implications for magma evolution and Cu–Mo mineralization. Int. Geol. Rev. 57, 1239–1266.
Li, B., Jiang, S.Y., 2014b. Geochronology and geochemistry of Cretaceous Nanshanping alkaline rocks from the Zijinshan district in Fujian Province, South China: implications for crust–mantle interaction and lithospheric extension. J. Asian Earth Sci. 93, 253–274.
Li, Z.X., Li, X.H., 2007. Formation of the 1300-km-wide intracontinental orogen and postorogenic magmatic province in Mesozoic South China: a flat-slab subduction model. Geology 35, 179–182.
Li, P.J., Li, H.Y., 2015. Geochronological, sedimentary, structural, and metallogenic characteristics of Southeast China during the Mesozoic: a general review. Int. J. Geosci. 6, 1032–1047.
Li, P.J., Yu, X.Q., Li, H.Y., Zhou, X., 2013a. Jurassic–cretaceous tectonic evolution of Southeast China: geochronological and geochemical constraints of Yanshanian granitoids. Int. Geol. Rev. 55, 1202–1219.
Li, B., Zhao, K.D., Yang, S.Y., Dai, B.Z., 2013b. Petrogenesis of the porphyritic dacite from Ermiaogou Cu-Au deposit in Zijinshan ore field and its metallogenetic implications. Acta Petrol. Sin. 29, 4167–4185 (in Chinese with English abstract).
Li, B., Zhao, K.D., Zhang, Q., Xu, Y.M., Zhu, Z.Y., 2015. Petrogenesis and geochemical characteristics of the Zijinshan granitic complex from Fujian Province, South China. Acta Petrol. Sin. 31, 811–828 (in Chinese with English abstract).
Liang, H.Y., Campbell, I.H., Allen, C., Sun, W.D., Liu, C.Q., Yu, H.X., Xie, Y.W., Zhang, Y.Q., 2006. Zircon Ce^{4+}/Ce^{3+} ratios and ages for Yulong ore-bearing porphyries in eastern Tibet. Mineral. Deposita 41, 152–159.
Liang, Q.L., Jiang, S.H., Wang, S.H., Li, C., Zeng, F.G., 2012. Re–Os dating of molybdenite from the Luoboling porphyry Cu–Mo deposit in the Zijinshan orefield of Fujian Province and its geological significance. Acta Geol. Sin. 86, 1113–1118 (in Chinese with English abstract).
Liang, Q.L., Jiang, S.H., Bai, D.M., Wang, S.H., 2015. Sources of ore-forming materials of epithermal deposits in Zijinshan orefield in Fujian Province: evidence from H, O, S and Pb isotopes. Mineral Deposits 34, 533–546 (in Chinese with English abstract).
Lin, Q.S., 2001. On the characteristics and genesis of the Yueyang silver polymetallic deposit in Wuping County, Fujian Province. Geol. Fujian 25, 82–88 (in Chinese with English abstract).
Lin, S.P., Liu, S., Wang, C.L., Huang, W.T., Li, Z.J., Wang, C.Z., Qi, J.P., Liang, H.Y., 2012. Locating the cryptoexplosion center at ermiaogou Cu polymetallic deposit in the zijin ore field and its geological implication. Geotecton. Metallog. 36, 450–456 (in Chinese with English abstract).
Liu, X.D., Hua, R.M., 2005. 40Ar/39Ar dating of adularia from the Bitian gold-silver-copper deposit, Fujian Province. Geol. Rev. 51, 151–155 (in Chinese with English abstract).
Liu, Y.S., Hu, Z.C., Gao, S., Guenther, D., Xu, J., Gao, C.G., Chen, H.H., 2008. In situ analysis of major and trace elements of anhydrous minerals by LA-ICP-MS without applying an internal standard. Chem. Geol. 257, 34–43.
Liu, Q., Yu, J.H., Su, B., Wang, Q., Tang, H.F., Xu, H., Cui, X., 2011. Discovery of the 187 Ma granite in Jincheng area, Fujian Province: constraint on early Jurassic tectonic evolution of southeastern China. Acta Petrol. Sin. 27, 3575–3589 (in Chinese with English abstract).
Ludwig, K.R., 2003. Isoplot/Ex, version 3.0: A geochronological toolkit for Microsoft Excel. Geochronology Center, Berkeley, Special Publication.
Machado, N., Simonetti, A., 2001. U-Pb dating and Hf isotopic composition of zircon by laser-ablation-MC-ICP-MS. In: Sylvester, P. (Ed.), Mineral. Assoc. Canada, Special Publication, pp. 121–146.
Mao, J.R., Tao, K.Y., Li, J.Y., Xie, F.G., Xu, N.Z., 2002. Geochronology and geochemical characteristics in Late Mesozoic Sifang pluton, southwestern Fujian, and their significance. Acta Petrol. Sin. 18, 449–458 (in Chinese with English abstract).
Mao, J.R., Xu, N.Z., Hu, Q., Xing, G.F., Yang, Z.L., 2004. The Mesozoic rock-forming and ore-forming processes and tectonic environment evolution in Shanghang-Datian region, Fujian. Acta Petrol. Sin. 20, 285–296 (in Chinese with English abstract).
Mao, J.W., Cheng, Y.B., Chen, M.H., Franco, P., 2013. Major types and time–space distribution of Mesozoic ore deposits in South China and their geodynamic settings. Mineral. Deposita 48, 267–294.
McInnes, B.I.A., Cameron, E.M., 1994. Carbonated, alkaline hybridizing melts from a sub-arc environment: mantle wedge samples from the Tabar-Lihir-Tanga-Feni arc, Papua New Guinea. Earth Planet. Sci. Lett. 122, 125–141.
Meng, L.F., Li, Z.X., Chen, H.L., Li, X.H., Wang, X.C., 2012. Geochronological and geochemical results from Mesozoic basalts in southern South China Block support the flat-slab subduction model. Lithos 132, 127–140.
Middelburg, J.J., Van der Weijden, C.H., Woittiez, J.R.W., 1988. Chemical processes affecting the mobility of major, minor and trace elements during weathering of granitic rocks. Chem. Geol. 68, 253–273.
Müller, D., Rock, N.M.S., Groves, D.I., 1992. Geochemical discrimination between shoshonitic and potassic volcanic rocks in different tectonic settings: a pilot study. Mineral. Petrol. 46, 259–289.
Mungall, J.E., 2002. Roasting themantle: slabmelting and the genesis of major Au and Aurich Cu deposits. Geology 30, 915–918.
Muñoz, M., Charrier, R., Fanning, C.M., Maksaev, V., Deckart, K., 2012. Zircon trace element and O-Hf isotope analyses of mineralized intrusions from El Teniente ore deposit, Chilean Andes: constraints on the source and magmatic evolution of porphyry Cu-Mo related magmas. J. Petrol. 1091–1122.
Pearce, J.A., Peate, D.W., 1995. Tectonic implications of the composition of volcanic arc magmas. Annu. Rev. Earth Planet. Sci. 23, 251–285.
Rapp, R.P., Watson, E.B., 1995. Dehydration melting of metabasalt at 8–32 kbar, implications for continental growth and crust-mantle recycling. J. Petrol. 36, 891–931.
Rapp, R.P., Watson, E.B., Miller, C.F., 1991. Partial melting of amphibolite/eclogite and the origin of Archaean trondhjemites and tonalites. Precambrian Res. 51, 1–25.
Shirey, S.B., Walker, R.J., 1995. Carius tube digestion for low-blank Rhenium-Osnium analysis. Anal. Chem. 67, 2136–2141.
Shu, X.J., Wang, X.L., Sun, T., Chen, W.F., Shen, W.Z., 2013. Crustal formation in the Nanling Range, South China Block: Hf isotope evidence of zircons from Phanerozoic granitoids. J. Asian Earth Sci. 74, 210–224.
So, C.S., Zhang, D.Q., Yun, S.T., Li, D.X., 1998. Alteration mineralization zoning and fluid inclusions of the high sulfidation epithermal Cu-Au mineralization at Zijinshan, Fujian province, China. Econ. Geol. 93, 961–980.
Sobolev, S.V., Babeyko, A.Y., 2005. What drives orogeny in the Andes. Geology 33, 617–620.
Soderlund, U., Patchett, P.J., Vervoort, J.D., Isachsen, C.E., 2004. The ^{176}Lu decay constant determined by Lu-Hf and U-Pb isotope systematics of Precambrian mafic intrusions. Earth Planet. Sci. Lett. 219, 311–324.
Sun, S.S., McDonough, W.F., 1989. Chemical and isotopic systematics of oceanic basalts: implications for mantle composition and processes. Geol. Soc. Spec. Publ. 42, 313–345.
Sun, Y.L., Zhou, M.F., Sun, M., 2001. Routin Os analysis by isotope dilution inductively coupled plasma mass spectrometry: OsO_4 in water solution gives high sensitivity. J. Anal. At. Spectrom. 26, 345–349.
Sun, W.D., Ding, X., Hu, Y.H., Li, X.H., 2007. The golden transformation of the Cretaceous plate subduction in the west Pacific. Earth Planet. Sci. Lett. 262, 533–542.
Sun, W.D., Ling, M.X., Wang, F.Y., Ding, X., Hu, Y.H., Zhou, J.B., Yang, X.Y., 2008. Pacific plate subduction and Mesozoic geological event in Eastern China. Bull. Mineral. Petrol. Geochem. 27, 218–225 (in Chinese with English abstract).
Sun, Y.L., Xu, P., Li, J., He, K., Chu, Z.Y., Wang, Y., 2010. A practical method for determination of molybdenite Re-Os age by inductively coupled plasma-mass spectrometry combined with Carius tube-HNO3 digestion. Anal. Methods 2, 575–581.
Tchameni, R., Mezger, K., Nsifa, N.E., Pouclet, A., 2001. Crustal origin of Early Proterozoic syenites in the Congo Craton (Ntem Complex), South Cameroon. Lithos 57, 23–42.
Upadhyay, D., Raith, M.M., Mezger, K., Hammerschmidt, K., 2006. Mesoproterozoic rift-related alkaline magmatism at Elchuru, Prakasam Alkaline Province, SE India. Lithos 89, 447–477.
Villagómez, D., Spikings, R., Magna, T., Kammer, A., Winkler, W., Beltrán, A., 2011. Geochronology, geochemistry and tectonic evolution of the Western and Central cordilleras of Colombia. Lithos 125, 875–896.
Wang, Z.H., Lu, H.F., 1997. A preliminary discussion on the research of lithosphere tectonic evolution. Geol. J. China Univ. 3, 118–127.
Wang, Q., Xu, J.F., Jian, P., Bao, Z.W., Zhao, Z.H., Li, C.F., Xiong, X.L., Ma, J.L., 2006. Petrogenesis of adakitic porphyries in an extensional tectonic setting, Dexing, South China: implications for the genesis of porphyry copper mineralization. J. Petrol. 47, 119–144.
Wendt, I., Carl, C., 1991. The statistical distribution of the mean squared weighted deviation. Chem. Geol. Isot. Geosci. Sect. 86, 275–285.
Whitney, D.L., Evans, B.W., 2010. Abbreviations for names of rock-forming minerals. Am. Mineral. 95, 185–187.
Winchester, J.A., Floyd, P.A., 1977. Geochemical discrimination of different magma series and their differentiation products using immobile elements. Chem. Geol. 20, 325–343.
Wu, C., Chen, H.Y., Hollings, P., Xu, D.R., Liang, P., Han, J.S., Xiao, B., Cai, K.D., Liu, Z.J., Qi, Y.K., 2015. Magmatic sequences in the Halasu Cu Belt, NW China: trigger for the Paleozoic porphyry Cu mineralization in the Chinese Altay–East Junggar. Ore Geol. Rev. 71, 373–404.
Xu, X., O'Reilly, S.Y., Griffin, W.L., Wang, X., Pearson, N.J., He, Z., 2007. The crust of Cathaysia: age, assembly and reworking of two terranes. Precambrian Res. 158, 51–78.
Yang, W.B., Niu, H.C., Shan, Q., Sun, W.D., Zhang, H., Li, N.B., Jiang, Y.H., Yu, X.Y., 2014. Geochemistry of magmatic and hydrothermal zircon from the highly evolved Baerzhe alkaline granite: implications for Zr-REE-Nb mineralization. Mineral. Deposita 49, 451–470.
Yu, B., Pei, R.F., Qiu, X.P., Chen, J.H., Li, D.P., Zhang, W.H., Liu, W.Y., 2013. The evolution series of Mesozoic magmatic rocks in the Zijinshan Orefield, Fujian Province. Acta Geol. Sin. 34, 437–446 (in Chinese with English abstract).
Yuan, H.L., Gao, S., Liu, X.M., Li, H.M., Gunther, D., Wu, F.Y., 2004. Accurate U-Pb age and trace element determinations of zircon by laser ablation-inductively coupled plasma-mass spectrometry. Geostand. Geoanal. Res. 28, 353–370.
Zhang, D., 2014. Discussions on features of Mesozoic thrust-fault belts and relationship between thrust-fault belts and magmatism in Southwestern Fujian and adjacent regions (Ph.D. Thesis) China University of Geosciences, Beijing.
Zhang, D.Q., Li, D.X., Zhao, Y.M., Wang, W.G., Gu, G.X., 1996. The Wuziqilong copper deposit: the deformed upper part of a porphyry copper deposit. Mineral Deposits 15, 109–122 (in Chinese with English abstract).

Zhang, D.Q., Li, D.X., Feng, C.Y., Dong, Y.J., 2001. The temporal and spatial framework of the Mesozoic magmatic system in Zijinshan area and its geological significance. Acta Geosci. Sin. 22, 403–408 (in Chinese with English abstract).
Zhang, D.Q., She, H.Q., Li, D.X., Feng, C.Y., 2003. The porphyry-epithermal metallogenic system in the Zijinshan region, Fujian province. Acta Geol. Sin. 77, 253–261 (in Chinese with English abstract).
Zhang, D.Q., Feng, C.Y., Li, D.X., She, H.Q., Dong, Y.J., 2005. The evolution of ore-forming fluid in the porphyry-epithermal metallogenic system of Zijinshan area. Acta Geosci. Sin. 26, 127–136 (in Chinese with English abstract).
Zhao, X.L., 2007. The geochronology petrography and geochemical characteristics of Mesozoic granitoids from Shanghang area in SW Fujian and their implications (Master dissertation) Chinese Academy of Geological Sciences, Beijing, pp. 1–57 (in Chinese with English abstract).
Zhao, X.L., Mao, J.R., Chen, R., Xu, N.Z., Zeng, Q.T., Ye, H.M., 2007. Zircon SHRIMP age and geochemical characteristics of the Caixi pluton in southwestern Fujian province. Acta Petrol. Mineral. 26, 223–231 (in Chinese with English abstract).
Zhong, J., 2014. Temporal and Spatial evolution of the Zijinshan porphyry-epithermal magmatic and mineralization system, Fujian Province (Ph.D. Thesis) Peking University, Beijing.
Zhong, J., Chen, Y.J., Chen, J., Li, J., Qi, J.P., 2011. Fluid inclusion study of the Luoboling porphyry Cu–Mo deposit in the Zijinshan ore field, Fujian province. Acta Petrol. Sin. 27, 1410–1424 (in Chinese with English abstract).
Zhong, J., Chen, Y.J., Pirajno, F., Chen, J., Li, J., Qi, J.P., Li, N., 2014. Geology, geochronology, fluid inclusion and H–O isotope geochemistry of the Luoboling porphyry Cu–Mo deposit, Zijinshan Orefield, Fujian Province, China. Ore Geol. Rev. 57, 61–77.
Zhou, Q., 2011. Petrogenesis and metallogeny for the Dexing porphyry copper deposit (Ph.D. Thesis) Nanjing University, Nanjing.
Zhou, X.M., Li, W.X., 2000. Origin of Late Mesozoic igneous rocks in Southeastern China: implications for lithosphere subduction and underplating of mafic magmas. Tectonophysics 326, 269–287.
Zhou, X.M., Sun, T., Shen, W.Z., Shu, L.S., Niu, Y.L., 2006. Petrogenesis of Mesozoic granitoids and volcanic rocks in South China: a response to tectonic evolution. Episodes 29, 26–33.
Zijin Mining Group Co., 2014. Detailed investigation plan for the Southeast Ore Segment of the Zijinshan mineral deposit in 2014. Unpublished report. (in Chinese).